Author Manuscript

Author Manuscript

Author Manuscript

Author Manuscript

HHS Public Access

Author manuscript

Dev Cell. Author manuscript; available in PMC 2024 July 17.

Published in final edited form as:

Dev Cell. 2024 March 11; 59(5): 661–675.e7. doi:10.1016/j.devcel.2024.01.005.

PUF partner interactions at a conserved interface shape the RNA binding landscape and cell fate in *Caenorhabditis elegans*

Brian H. Carrick[1,*], **Sarah L. Crittenden**[1], **Fan Chen**[2,4], **MaryGrace Linsley**[1], **Jennifer Woodworth**[1,5], **Peggy Kroll-Conner**[1], **Ahlan S. Ferdous**[1,6], **Sündüz Keleş**[2,3], **Marvin Wickens**[1,*], **Judith Kimble**[1,7,*]

[1]Department of Biochemistry, University of Wisconsin-Madison, Madison, WI 53706, USA

[2]Department of Statistics, University of Wisconsin-Madison, Madison, WI 53706, USA

[3]Department of Biostatistics and Medical Informatics, University of Wisconsin-Madison, Madison, WI 53706, USA

[4]Present address: Google LLC, New York, NY 10011, USA

[5]Present address: Medical College of Wisconsin-Central Wisconsin, Wausau, WI 54401, USA

[6]Present address: Department of Biology, University of Washington-Seattle, Seattle, WI 98195, USA

[7]Lead Contact

Summary

Protein-RNA regulatory networks underpin much of biology. *C. elegans* FBF-2, a PUF RNA-binding protein, binds over 1000 RNAs to govern stem cells and differentiation. FBF-2 interacts with multiple protein partners via a key tyrosine, Y479. Here we investigate the *in vivo* significance of partnerships using a Y479A mutant. Occupancy of the Y479A mutant protein increases or decreases at specific sites across the transcriptome, varying with RNAs. Germline development also changes in a specific fashion: Y479A abolishes one FBF-2 function – the sperm to oocyte cell fate switch. Y479A effects on the regulation of one mRNA, *gld-1*, are critical to this fate change, though other network changes are also important. FBF-2 switches from repression to activation of *gld-1* RNA, likely by distinct FBF-2 partnerships. The role of RNA-binding protein partnerships in governing RNA regulatory networks will likely extend broadly, as such partnerships pervade RNA controls in virtually all metazoan tissues and species.

[*]Authors for correspondence: jekimble@wisc.edu, wickens@biochem.wisc.edu, bcarrickresearch@gmail.com.

Author Contributions

Conceptualization, B.H.C., S.L.C.; Formal Analysis, B.H.C., S.L.C., F.C.; Investigation, B.H.C., S.L.C., F.C., M.L., J.W., A.S.F; Resources, B.H.C., S.L.C., M.L., J.W., P.K.C., A.S.F.; Data Curation, B.H.C., F.C.; Writing – Original Draft, B.H.C., S.L.C., M.W., J.K.; Writing – Review & Editing, B.H.C., S.L.C, F.C., M.L., J.W., P.K., M.W., J.K.; Funding Acquisition, B.H.C., M.W., J.K.

Publisher's Disclaimer: This is a PDF file of an unedited manuscript that has been accepted for publication. As a service to our customers we are providing this early version of the manuscript. The manuscript will undergo copyediting, typesetting, and review of the resulting proof before it is published in its final form. Please note that during the production process errors may be discovered which could affect the content, and all legal disclaimers that apply to the journal pertain.

Declaration of Interests

The authors declare no competing interests.

Author Manuscript Author Manuscript Author Manuscript Author Manuscript

Graphical Abstract

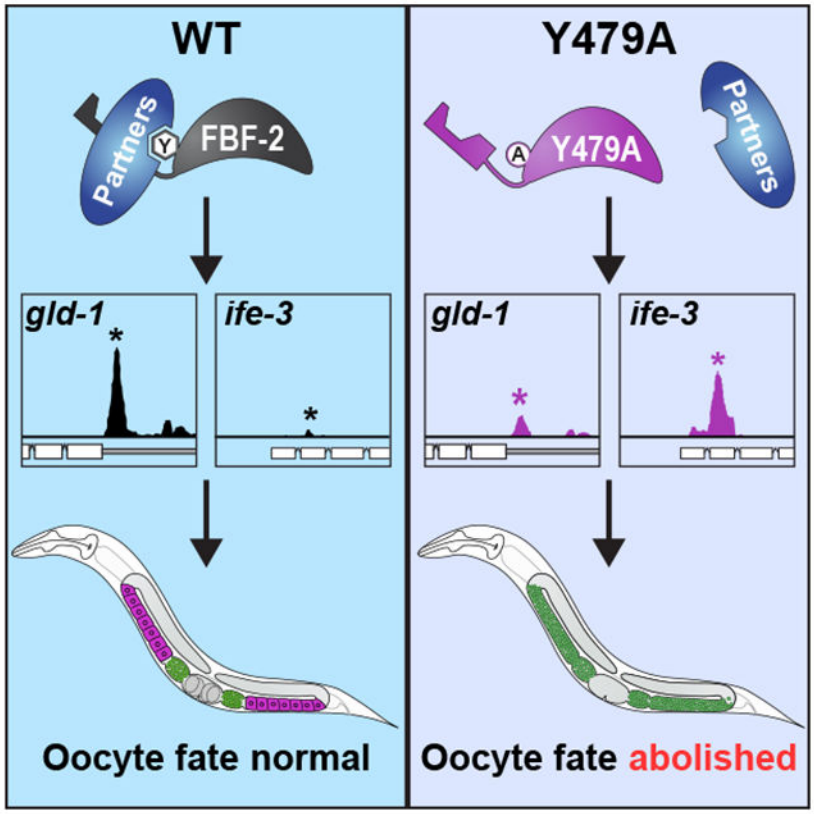

eTOC blurb

Carrick et al. demonstrate that a conserved PUF/PUM partner binding interface on FBF-2 defines its RNA binding landscape (transcriptome-wide sites of FBF-2 occupancy) and regulation of cell fate. Moreover, they show that the FBF-2 partner binding interface can drive a spatially patterned switch from RNA repression to activation.

Keywords

C. elegans; FBF-2; PUF/PUM RNA binding protein; PUF/PUM partner proteins; eCLIP; RNA binding landscape; *gld-1* RNA; FBF binding elements; germline stem cells; sperm/oocyte fate decision

Introduction

Protein-RNA networks regulate a wide range of biological processes[1–4]. One family of RNA-binding proteins (RBPs), the PUF (for Pumilio/PUM and FBF) family, is exemplary in their central role in the control of such networks[5–8]. PUF proteins have conserved roles in stem cells and neurons, and when aberrant, can cause human disease, including cancer and epilepsy[9–15]. PUF proteins commonly bind 100s to 1000s of RNAs[3,16–22], with several validated as functional targets *in vivo* (e.g. *gld-1, fem-3* in *C. elegans*[23,24]). PUF proteins

Author Manuscript Author Manuscript Author Manuscript Author Manuscript

collaborate with protein “partners” (Figure 1A). Some of those partners bind to RNA themselves and can influence RNA binding specificity *in vitro* (e.g. CPEB[25,26]); others modify RNA and thereby specify regulatory mode (e.g. Ccr4-Not deadenylase complex[27–29]). PUF “partnerships” are thus central to PUF-RNA networks, expanding their reach and versatility[25,30–32]. A major challenge now is to understand how these partnerships shape PUF-RNA networks *in vivo* and regulate development.

To address this challenge, we focus on *C. elegans* FBF-2, a paradigmatic PUF protein with multiple partner proteins (see below) and a well-established RNA network[19]. FBF-2 and FBF-1, its nearly identical and largely redundant counterpart, have two major biological roles: self-renewal of germline stem cells (GSCs) and regulation of the sperm to oocyte (s/o) cell fate switch in hermaphrodites[23,24]. FBF-2 binds to >1000 mRNAs of which most overlap with FBF-1 and >400 overlap with PUM2 targets in humans, suggesting conservation of their RNA networks[19,33]. *In vitro*, FBF-1 and FBF-2 (collectively termed FBF) bind to the same consensus FBF binding element (FBE) with nanomolar affinity[19,34–36]; this and other related elements mediate their binding *in vivo*[17–19]. *In vivo*, FBF is best known to repress mRNA expression[18,23,24,37,38], but may also activate it[39,40].

Like all classical PUF proteins, FBF-2 possesses an N-terminal intrinsically disordered region and a C-terminal RNA binding domain (RBD) with eight PUF repeats[36] (Figures 1B and 1C). Also like all classical metazoan PUF proteins, the crescent-shaped RBD of FBF-2 contacts RNA on its inner surface (Figure 1B, blue residues)[41,42] and partner proteins on its outer surface. Most relevant to this work is the R7/R8 loop, which resides between PUF repeats 7 and 8 (Figure 1B, green residues) and provides a partner-binding interface that is conserved from nematodes to humans (Figure 1D, Tables S1 and S2)[26,32,43–49]. For example, human and worm Cytoplasmic Polyadenylation Element Binding proteins (CPEBs) and fly Nanos all bind at the R7/R8 loop, as assayed *in vitro* and in yeast[26,50,51] (Figure 1D, Tables S1 and S2). Here we focus on the R7/R8 loop to investigate the role of PUF partnerships *in vivo*.

Within the FBF-2 R7/R8 loop, a single tyrosine residue Y479, is critical for binding to several partners (Figure 1B, purple residue). Thus, an alanine substitution of this key tyrosine, Y479A, abrogates interactions for three distinct partners, LST-1, GLD-3 and CPB-1, when tested either *in vitro* or yeast[26,32,43] (Figure 1D). *In vitro*, Y479A also abrogates an intramolecular interaction with the FBF-2 C-terminal ‘tail’, which autoinhibits RNA binding by increasing the FBF-2 off-rate[44] (Figure 1D). Each of the Y479-dependent interactors harbors at least one PUF-interacting motif (PIM) that binds to the R7/R8 loop via Y479[31,32,43,44,51]. Other partners can bind at different locations. Examples include CSR-1/AGO, which binds at the R4/R5 loop[52] and the Ccr4-Not complex, which likely binds via the intrinsically disordered N-terminal region[53–55]. The FBF-2 sites where other partners bind have not yet been determined experimentally. Genetic analyses demonstrate that partners can regulate GSC self-renewal (LST-1, SYGL-1) and the sp/oo switch (NOS-3) (Figure 1D, Tables S1 and S2). FBF-2 partnerships thus continue to grow in number and complexity.

Author Manuscript Author Manuscript Author Manuscript Author Manuscript

To investigate how partnerships shape PUF-RNA networks, we use the FBF-2 Y479 residue as a unique entrée to understand the *in vivo* significance of PUF partnerships. We generate Y479A mutant nematodes to abrogate PUF partnerships and find dramatic changes to both the *in vivo* FBF-2 RNA binding landscape and germline function. Among the 100's of RNAs with altered Y479A occupancy, we focus on the *gld-1* mRNA to learn how its FBF-2 binding elements affect expression of the GLD-1 protein and germline fate. This single RNA accounts for most, but not all, Y479A effects on germline function. The combination of genome-wide and gene-specific approaches helps to explain how large-scale transcriptomic regulation can produce specific biological effects.

Results

Y479 partners with LST-1 *in vivo*

We replaced Y479 with alanine in the endogenous *fbf-2* gene to test its *in vivo* role in shaping the RNA-binding landscape (Figure 1C). Y479A mutants were fertile, and expression of Y479A protein was comparable to wild-type (Figures S1A–S1D). The Y479A fertility mimics that of an *fbf-2* null mutant, which has a normally organized and functional germline due to the presence of wild-type FBF-1, the redundant counterpart of FBF-2[56]. We thus could compare the Y479A and wild-type RNA binding landscapes in phenotypically comparable animals.

To validate Y479 being critical for FBF-2 partnerships *in vivo*, we tested its role on the FBF-2:LST-1 interaction. This particular partnership had been validated by co-immunoprecipitation (coIP) of wild-type proteins[31] and its dependence on Y479 had been demonstrated *in vitro*[32]. We used nematodes carrying FLAG-tagged FBF-2 and V5-tagged LST-1 for coIPs. As expected, wild-type FBF-2^{FLAG} coIP'd with LST-1^{V5} (Figure S1Ebut FBF-2(Y479A)^{FLAG} and LST-1^{V5} did not (Figure S1E). Therefore, as expected, Y479A abrogates the FBF-2:LST-1 partnership in nematodes. This mutation is thus likely to affect other Y479-dependent interactions as well.

LST-1 is arguably the best established Y479-dependent FBF-2 partner, but others are known (Figure 1D) [26,32,43–49] and yet others are suspected (Table S1). We predicted that Y479-dependent partners would bind to FBF-2 in a manner similar to LST-1, and tested this prediction with AlphaFold. In crystal structures, short intrinsically disordered LST-1 peptides and the FBF-2 C-terminal tail interact with the FBF-2 R7/R8 loop via PUF-interacting motifs (PIMs) (Figure S2A)[32,44,57]. Remarkably, the top ranked AlphaFold predictions revealed that all known, as well as all suspected, Y479-dependent partners (LST-1, SYGL-1, NOS-3, GLD-3, CPB-1, and DAZ-1) interact similarly at the R7/R8 loop (Figure S2B) and do so via PIM-like sequences (Figure S2C). In contrast, partners expected to bind outside the R7/R8 loop failed to fold with the FBF-2 RBD (Figure S2D). These predictions suggest that Y479A likely abrogates multiple interactions with partner proteins *in vivo*, when taken together with *in vitro* results (Figure 1D) and *in vivo* LST-1:FBF-2 coIP results (Figure S1E).

Author Manuscript Author Manuscript Author Manuscript Author Manuscript

Key tyrosine in R7/R8 loop modulates FBF-2 RNA-binding landscape

To investigate Y479A effects on the FBF-2 RNA-binding landscape, we used eCLIP (enhanced CrossLinking and ImmunoPrecipitation)[58]. Living animals (wild-type or Y479A) were UV-irradiated and lysed, FBF-2 immunoprecipitated (Figure S3A) and bound RNAs identified by sequencing (Figure 1E). From four biological replicates of each genotype, reproducible peaks were identified with standard programs[58]. “Peak heights” (normalized read counts under each peak assessed as fragments per kilobase mapped, FPKM) provided a measure of *in vivo* FBF-2 binding occupancy at sites in target RNAs[59]. The peak heights correlated well among all wild-type FBF-2 replicates and also among all Y479A replicates (Rho values ~0.9-0.99), but correlation was lower between wild-type and Y479A (Rho values ~0.7-0.85, Figure S3B). The eCLIP datasets of wild-type FBF-2 substantially overlapped with published iCLIP datasets, including both mRNAs and lncRNAs[19] (Figure S3C). Most peaks mapped to 3’UTRs (Figure S3D) and the most enriched motif was a consensus FBF binding element (FBE) (UGUNNNAU; “N” denotes any base) (Figure S3D). These eCLIP datasets thus provide high-quality lists of bound RNAs and define the RNA-binding landscapes of wild-type FBF-2 and Y479A.

To detect differences between wild-type and Y479A in RNA occupancy, we used DiffBind[60]. Peaks were designated as different if their heights had a $\log_2$ fold change of ≥ 0.5 or ≤ -0.5 and their False Discovery Rate was ≤ 0.01 (Figure 1F). Among 2,702 peaks identified, three categories emerged: (1) no significant difference between wild-type FBF-2 and Y479A (2260 peaks in 1207 RNAs), (2) significantly “lower” in Y479A (127 peaks in 82 RNAs) and (3) significantly “higher” in Y479A (315 peaks in 249 RNAs) (Figure 1F and Table S3). In addition, 141 RNAs possessed peaks in more than one category, i.e. an RNA can have multiple peaks, and these peaks do not have the same Y479-dependent effects (Figure 1G, circle intersections). The changes are therefore peak-specific rather than RNA-specific. We note that average wild-type peak heights differed for each category. Peaks lower in Y479A had the highest average peak height in wild-type (Figures 1H, S3E and S3F), suggesting Y479-dependence at FBEs with highest FBF-2 occupancy *in vivo*. Importantly, peak height differences did not correlate with RNA abundance (Figure 1I). We conclude that Y479 is required to modulate a subset of targets in the RNA-binding landscape.

Y479A shifts RNA-binding from 3’UTRs to coding sequences

To identify RNA features underlying the differential binding of wild-type and Y479A, we analyzed Y479A peaks in each category, with representative examples provided for illustration (Figures 2A–2C). The consensus FBE (UGUNNNAU)[34] was enriched under peaks in all categories (Figures 2D–2F). Motifs for other RNA-binding proteins were not found, assessed by Tomtom in the MEME suite. Table S3 lists peaks with a consensus FBE or a shorter ‘compact/cFBE’ (UGUNNAU)[20,32]. Searches for enriched GO terms confirmed previous GO analyses[19,20] and found no striking difference between categories (Figures S4A–S4C). The most striking difference in this analysis was that peak positions and peak heights differed by category: Most peaks “lower” in Y479A mapped to 3’UTRs (94%) (Figure 2H) and their wild-type peak heights were higher than average (Figures 1G and S3E). By contrast, most peaks “higher” in Y479A mapped to coding sequences (CDS)

Author Manuscript Author Manuscript Author Manuscript Author Manuscript

(61%) (Figure 2I) and their wild-type peak heights were lower than average (Figures 1H and S3E). One explanation is that loss of Y479A from high-occupancy sites in 3'UTRs frees the protein to occupy sites in CDSs and 5'UTRs.

Although Y479 does not contact RNA (Figure 1B), we asked if differences in intrinsic RNA binding affinity might explain the distinct occupancies of wild-type and Y479A proteins. In yeast three hybrid assays, wild-type and Y479A bind with similar apparent affinities to one particular FBE, "FBEa" in the *gld-1* 3'UTR[26], yet by eCLIP, the *in vivo* occupancies of this same FBE were significantly different (Y479A ~3 fold lower peak height than wild-type, FDR = $1.6x10^{-42}$) (Figure 2B and Table S3). To measure *in vitro* RNA affinities with purified components, we used fluorescence polarization. Purified, recombinant FBF-2 and Y479A proteins (Figure S5A) were incubated with fluorescein labeled RNAs harboring a wild-type or mutant FBE (Figure S5B). Affinities were assayed for three RNAs (*daz-1, gld-1* and *ife-3*), each in a different category (Figures 2A–2C). Wild-type FBF-2 and Y479A proteins bound with similar apparent K_dS to each RNA (Figures 2J–2L). Thus, Y479A does not measurably affect intrinsic RNA binding affinity, suggesting that, *in vivo*, interactions at the R7/R8 loop modify FBF-2 occupancies at specific sites.

Y479A retains repressive activity

FBF-2 is thought to repress RNAs, either by recruiting the CCR4/Not complex or sequestering RNA to perinuclear granules[40,61,62]. As Y479A has little effect on FBF-2 abundance or granule localization (Figures S1A–S1D), we tested its RNA regulatory activity, using an mRNA-protein tethering strategy that takes advantage of high affinity binding of λN22 peptide to BoxB RNA elements[63,64]. We therefore tagged wild-type FBF-2 and Y479A with λN22 peptide and tested their regulatory activities with a GFP reporter carrying BoxB elements in its 3'UTR[65] (Figure 3A). As a readout, we scored GFP fluorescence intensity in the germline (Figures 3B and 3C). For both wild-type FBF-2 and Y479A, GFP intensity was high when untethered (Figures 3D and 3G), and reduced when tethered (Figures 3E and 3H); quantitation confirmed that they have comparable RNA repressive activities (Figures 3F and 3I). Moreover, both wild-type FBF-2 and Y479A co-immunoprecipitated with the scaffold protein of the Ccr4-Not complex, Not1/NTL-1 (Figure 3J). Therefore, the FBF-2 interaction with Not1 is not Y479A-dependent. We conclude that wild-type and Y479A FBF-2 proteins have comparable RNA repressive activities and comparable interactions with Ccr4-Not.

FBF-2 occupancy affects target mRNA expression

To ask if Y479A changes to FBF-2 occupancy affect RNA expression, we stained gonads for proteins made from target mRNAs in each category (Figures 4A–4F), and quantitated protein abundance as a function of position in the distal gonad (Figures 4G–4I). Epitope-tags were inserted to visualize DAZ-1 and IFE-3 proteins, and α-GLD-1 antibodies were used to visualize GLD-1. For *daz-1*, where wild-type and Y479A eCLIP peaks were equivalent (Figure 2A and Table S3), DAZ-1 protein abundance was essentially the same in wild-type and Y479A gonads (Figures 4A, 4D and 4G). For *gld-1*, where Y479A peaks were dramatically lower than wild-type (Figure 2B and Table S3), GLD-1 abundance (Figures 4B, 4E and 4H) mimicked that seen in *fbf-2* null mutants[66], suggesting that lower occupancy

Author Manuscript Author Manuscript Author Manuscript Author Manuscript

causes a loss of regulation. For *ife-3*, where the Y479A peak was higher than wild-type (Figure 2C and Table S3), IFE-3 abundance decreased in Y479A (Figures 4C, 4F, and 4I), suggesting that higher Y479A occupancy causes an aberrant increase in RNA repression. Thus, target RNAs are misregulated in Y479A, and their misregulation correlates with FBF-2 occupancy.

Y479A selectively abolishes one FBF-2 biological function

It was paradoxical that Y479A changed the FBF-2 RNA-binding landscape without affecting germline fate. A minor delay in meiotic entry was seen in Y479A mutants (Figure S6C), which was also seen in *fbf-2* null mutants[56], but otherwise the Y479A germlines were normal. However, FBF-2 defects are likely masked by its redundant counterpart FBF-1. FBF-1 and FBF-2 share three germline functions: they promote self-renewal in germline stem cells (GSCs)[23], the sperm to oocyte cell fate switch[24], and sperm function[48] (Figures 5A and 5B). All three functions are abolished in *fbf-1 fbf-2* double null mutants.

To ask if FBF-1 removal would reveal a more substantial Y479A defect, we examined *fbf-1(ø) fbf-2(Y479A)* double mutants, called “Y479A-only” for simplicity. Whereas fertile animals make sperm and then switch to oogenesis to generate self-progeny (Figure 5B), Y479A-only animals made sperm continuously over several days with no sign of oogenesis. The same sperm-only sterility was seen with an *fbf-2* transgene deleted for the entire R7/R8 loop and introduced into *fbf-1 (ø) fbf-2(ø)* mutants (Figure S6A). We confirmed the sperm-only phenotype in Y479A-only germlines with molecular markers. Wild-type gonads stained positively with both sperm- and oocyte-specific antibodies (Figure 5C), as did Y479A gonads that still had wild-type FBF-1 (Figure 5D). However, Y479A-only gonads stained positively for sperm but not for oocytes (Figure 5E). The single tyrosine, Y479, is thus vital to the sperm to oocyte cell fate switch.

We next asked whether Y479 affects other FBF-2 functions. GSCs were likely maintained in Y479A-only gonads because they were comparable in size to wild-type (compare Figure 5E to 5C) and had immature germ cells distally (Figure 5E). By contrast, germlines lacking both FBF-1 and FBF-2 are small and have no GSCs (Figure 5F). To test more rigorously for GSCs, we stained Y479A-only gonads for both a GSC-specific RNA (*lst-1*) and a hallmark proliferation protein, phospho-histone H3 (PH3), with positive results for both (Figure 5G and 5H). Sperm function was also normal when tested in Y479A-only males (Figure 5I and S6B). We conclude that the Y479A mutation abolishes one FBF-2 function, the sperm to oocyte cell fate switch, but leaves its other two functions intact.

FBF-2 regulation switches from *gld-1* RNA repression to *gld-1* RNA activation

Occupancy of wild-type FBF-2 was exceptionally high at sites in one particular RNA, the *gld-1* RNA (10% of total reads in eCLIP), and Y479A dramatically lowered that occupancy (Figure 2B). The *gld-1* RNA was also interesting because its GLD-1 protein product promotes germline differentiation, including the sperm to oocyte (s/o) fate switch[23,67,68]. To ask if a change to *gld-1* regulation might account for the Y479A-only s/o switch defect, we mutated the two canonical *gld-1* FBEs, both singly and together, in the endogenous gene (Figure 6A). These mutations disrupt binding of both FBF-1 and FBF-2[23]. Most

Author Manuscript Author Manuscript Author Manuscript Author Manuscript

single FBEa (97%) and FBEb (100%) mutants were fertile, but most FBEab double mutants were sterile (87%). The sterile FBEab mutants all failed in the s/o switch and some also failed to maintain GSCs (7%) (Figure 6B). By comparison, Y479A-only mutants were all sterile (100%) and all failed to switch (100%), but none lost their GSCs (0%). The FBEab and Y479A-only mutant phenotypes are thus similar but not identical. A change in *gld-1* regulation thus has a strong effect on the s/o switch, similar to the Y479A-only phenotype, but is not the whole story (see Discussion).

We next asked how *gld-1* FBE mutants affect expression of the GLD-1 protein. In wild-type, GLD-1 abundance was very low distally in GSCs, but increased more proximally as germ cells began differentiation (Figure 6C), as previously described[66,69]. In FBEa single mutants, GLD-1 abundance was higher than wild-type in GSCs, indicating a failure to repress expression (Figures 6C, upward arrow, and S7A), but in FBEb single mutants, GLD-1 was similar to wild-type (Figures 6C and S7A). Therefore, FBEa plays a larger role than FBEb in *gld-1* repression, consistent with its higher FBF-2 occupancy (Figure 6A). In FBEab double mutants, GLD-1 was again higher than normal distally in GSCs (Figures 6C, upward arrow, and S7A), but appeared lower than normal more proximally in differentiating daughters (Figures 6C and S7A), suggesting failures to repress distally and activate more proximally. These FBEab germlines made only sperm, and we were concerned that masculinization might affect GLD-1 expression. We therefore made the FBE mutants in a GFP:*gld-1* 3'UTR reporter transgene[70]. In this case, germlines were not masculinized, and animals were fertile. Nonetheless, expression changes were comparable in FBE mutants made in the endogenous gene and reporter (Figures 6C, S7B and S7C). FBE effects on GLD-1 expression are thus similar in spermatogenic and oogenic germlines – higher than normal distally and lower than normal more proximally. We conclude that the *gld-1* FBEs are required for spatial regulation of *gld-1* RNA expression.

We next examined the pattern of GLD-1 expression in Y479A-only gonads for comparison with the *gld-1* FBEab mutant. In Y479A-only, GLD-1 was higher than the control in GSCs (Figures 6D and 6E, upward arrow), and lower than the control more proximally (Figures 6D and 6E, downward arrow). The similarity of Y479A-only and FBEab effects on GLD-1 expression (Figures 6C, far right, and 6E) supports two conclusions. First, Y479A mimics the effect of eliminating FBF-2 binding to *gld-1* RNA, both in the presence of FBF-1 (Figure 4H) and the absence of FBF-1 (Figures 6D and 6E). Second, Y479A is defective for spatially distinct modes of *gld-1* regulation – repression in GSCs and activation upon differentiation.

Discussion

This work reveals the *in vivo* influence of Y479, a single tyrosine in FBF-2, on the molecular, biological and regulatory functions of this paradigmatic PUF protein. Y479 lies in a conserved protein-protein interaction interface that mediates multiple PUF partnerships. This region and Y479 in particular are essential for interactions with key FBF-2 partners both *in vitro*[26,32,43,51] (Figure 1D) and *in vivo* (this work). Our findings lead to several conclusions, with implications for PUF partnerships more broadly.

Author Manuscript Author Manuscript Author Manuscript Author Manuscript

Y479 plays a critical role in defining the FBF-2 RNA-binding landscape. This single residue is required to modulate FBF-2 occupancy at specific sites across the transcriptome, decreasing occupancy at some sites and increasing it at others. Other studies of RNA-binding proteins have identified single residue mutations that affect RNA binding specificity *in vivo*[71–75], but many of them alter intrinsic RNA binding affinity, protein abundance, or propensity to form condensates. By contrast, we found no detectable effect of Y479A on these properties, with affinity measured *in vitro* (Figures 2J–2L) and abundance and granule association assessed *in vivo* (Figures S1A–D). An independent *in vitro* assay using different conditions found that Y479A can increase K_d by reducing off-rate[44]. Regardless, the overarching conclusion is that Y479A *in vivo* changes FBF-2 occupancy on RNA targets (Figure 1F). Although most eCLIP peaks remained the same in Y479A, 20% of those peaks changed by 1.5-fold or more. These *in vivo* changes to the RNA-binding landscape were thus both significant and selective.

We propose models to explain how partnerships interacting via Y479 shape the FBF-2 RNA binding landscape (Figure 7). First, sites with unchanged occupancy in eCLIP may be bound by FBF-2 without a partner or with a partner that does not rely on Y479 for its FBF-2 interaction (Figure 7A). Moreover, interaction with the autoinhibitory C-terminal tail must not affect binding at these sites. Second, sites with decreased occupancy in Y479A may rely on a Y479-dependent partner to stabilize FBF-2 binding (Figure 7B). That partner might bind RNA itself or release the FBF-2 interaction with its autoinhibitory C-terminal tail, both of which have been demonstrated *in vitro*. For example, nematode CPEB and Drosophila Nanos bind RNA themselves and also enhance PUF binding to RNA[25,50,51], and LST-1 can release FBF-2 from its C-tail autoinhibition and thus strengthen FBF-2 binding to RNA[44]. Third, sites with higher occupancy in Y479A – for example those in coding regions – may rely in wild-type on a Y479-dependent partner to destabilize FBE occupancy or release C-terminal tail autoinhibition (Figure 7C) or those sites may take advantage of excess Y479A released from preferred sites moving to suboptimal sites (Figures 7B and 7C – dotted line). The mechanisms by which protein partners interact with FBF to mediate decreases and increases in occupancy likely depend on context of the FBE within the RNA and on expression or modification of the partners themselves. Effects of individual Y479-dependent partners on the RNA-binding landscape, as well as Y479-independent partners, remain a challenge for the future. Nonetheless, Y479A-induced changes show definitively that PUF partnerships have a broad influence on site-specific occupancy *in vivo*.

PUF proteins are well established as mRNA repressors[15,16,28,29,76,77], but they can also positively regulate RNAs[39,40,78]. Our work reveals that the FBF-2 regulation of *gld-1* switches from repression to activation and does so in a spatially regulated manner (Figure 7D). Moreover, this dynamic regulation relies on both *gld-1* FBEs (Figures 6C–6F) and Y479 at the FBF-2 partner interface (Figures 6G and 6H). Previous studies showed that PUF partners driving *gld-1* repression are localized more distally (e.g. LST-1, SYGL-1)[38,46], while those driving *gld-1* activation are localized more proximally (e.g. GLD-3)[47]. We propose that these repressive and activating partners stabilize FBF-2 occupancy with distinct effectors (e.g. LST-1 with Ccr4-Not deadenylase distally, GLD-3 with GLD-2 poly(A) polymerase proximally) (Figure 7D). By this model, loss of both types of partnerships in the Y479A mutant is predicted to lead to derepression distally and deactivation proximally.

Author Manuscript Author Manuscript Author Manuscript Author Manuscript

An analogous regulatory switch is also seen for yeast Puf3[78], suggesting that the ability to switch regulatory mode is widespread among PUFs and likely other RNA binding proteins (e.g. FMRP and DAZL[79,80]).

The biological effects of Y479 reveal its role in a subset of PUF functions. The Y479A mutant abolishes the sperm to oocyte (s/o) cell fate switch but not GSC self-renewal. One possible explanation is that differential target binding and resulting regulation creates biological specificity. For example, upregulation of *fem-3* RNA abolishes the s/o switch without affecting GSCs[81]. We find that *fem-3* FBEs had a lower FBF-2 occupancy in Y479A mutants, consistent with decreased repression. Conversely, downregulation of *ife-3* RNA abolishes the s/o switch[82], again without an effect on GSCs, and *ife-3* FBEs had a higher FBF-2 occupancy in Y479A mutants, consistent with increased repression. In addition, Y479A mis-regulates key targets, like *gld-1* (decreased occupancy in Y479A), involved in both GSC self-renewal and the s/o switch. The effects of increased GLD-1 in GSCs could be offset by normal regulation of other targets critical to GSC self-renewal[83–85]. These examples highlight roles of both individual RNAs and the network.

RNA binding proteins are implicated in a wide spectrum of human diseases[86–89]. Like Y479A, many disease alleles in RNA binding proteins map away from residues that bind RNA, and some map to predicted protein-protein interaction domains[12,14,86,87,90]. The principles revealed by Y479A analysis enable reconsideration of the sometimes enigmatic effects of RBP mutations in humans. As with the Y479A allele, mutations in other RBPs may cause disease by rewiring their RNA-binding network, leading to both loss of regulation of some RNAs, and gain of regulation of other RNAs. A recent study showed that disease-relevant alleles of human PUM altered PUM-partner interactions and led to disruptions in regulation of the PUF RNA network[14]. The importance of PUF proteins in human health and disease[12–14,90], and the existence of conserved PUF protein partners in humans, suggests that PUF partnerships will soon take center stage in understanding how human PUF functions are modulated and go awry.

Limitations of the Study

This work focused on FBF-2 partnerships acting at a specific residue lying within a conserved protein-protein interaction interface, but it did not distinguish among roles of individual Y479-dependent partners and it did not address roles of other FBF-2 protein-protein interaction interfaces. Our focus is on effects of full length FBF-2 and full length partners in their native context *in vivo*. *In vitro*, a peptide fragment of LST-1, which is a Y479-dependent partner, changed curvature of the FBF-2 RBD and modified its RNA binding affinity[46]. It is not known if those same changes occur *in vivo*. We suspect that Y479A does not affect FBF-2 structure because this key residue lies in a solvent-exposed, unstructured loop of the RBD. However, structure of Y479A mutant protein is unknown and we cannot rule out this possibility.

Author Manuscript Author Manuscript Author Manuscript Author Manuscript

STAR Methods

RESOURCE AVAILABILITY

Lead Contact—Further information and requests for resources and reagents should be directed to and will be fulfilled by the lead contact, Judith Kimble (jekimble@wisc.edu).

Materials availability—*C. elegans* strains generated in this study will be available from the CGC. Plasmids will be available from Addgene.

Data and code availability—eCLIP data have been deposited at GEO and are publicly available as of the date of publication under accession number GSE233561.

This paper does not report original code.

Any additional information required to reanalyze the data reported in this paper is available from the lead contact upon request.

EXPERIMENTAL MODEL AND STUDY PARTICIPANT DETAILS

Caenorhabditis elegans were maintained by on NGM seeded with OP50 with standard techniques[95] and grown at 20°C except where noted. Hermaphrodite animals were grown to 24 hours past the L4 stage unless otherwise noted. Strains used are listed in Key Resources Table.

METHOD DETAILS

CRISPR-Cas9 mediated gene editing—CRISPR-Cas9 alleles were created by co-CRISPR editing using a CRISPR/Cas9 RNA-protein complex[113–115]. Animals were injected with a mix containing a gene-specific crRNA (5 μM, IDT-Alt-R), unc-58 or dpy-10 crRNA (4 μM, IDT-Alt-R), tracRNA (4.5 μM, IDT), unc-58 or dpy-10 repair oligo (1 μM, IDT), gene-specific repair oligo (5 μM, IDT) and Cas9 protein (3 μM, glycerol free, IDT). F1 progeny of injected hermaphrodites were screened for edits by PCR, homozygosed, sequenced and outcrossed against wild-type prior to analysis. See Table S5 for guide RNA and repair template sequences.

mos1-mediated single-copy insertion (mosSCI)—The complete *fbf-2* genomic sequence (1.5 kb of the 5' upstream region, all exons and introns, and 1.1 kb of the 3' downstream region, plus an insert of 3xFLAG at the 5' end of the coding sequence was previously cloned into pCFJ151[116] to create pJK1726[20]. Y479 to T485 was deleted with site directed mutagenesis by PCR to create pJK2012 (3xFLAG:FBF-2(ΔR7 R8 loop). Transgene was inserted into the *ttTi5605* site on *LGIV* of strain EG8081 using the universal *mos1*-mediated single copy insertion (mosSCI) method[96] to generate *qSi364*. The presence of the transgene was verified by PCR and Sanger sequencing.

Structure prediction—FBF-2:partner structure predictions were created using the default parameters of ColabFold[117,118]. FBF-2 amino acids 121-632 were tested against the following; LST-1 (1-328), SYGL-1 (1-206), NOS-3 (192-681), GLD-3 (582-969), CPB-1 (1-200), DAZ-1 (1-498), DLC-1 (1-89), CSR-1 (557–993).

Author Manuscript Author Manuscript Author Manuscript Author Manuscript

eCLIP—eCLIP was carried out as described[58] (SOP v1.P 20151108, https://static-content.springer.com/esm/art%3A10.1038%2Fnmeth.3810/MediaObjects/41592_2016_BFnmeth3810_MOESM199_ESM.pdf) with modifications for worm growth and lysis described previously and below[20]. Paired end sequencing was performed on an Illumina NovaSeq 6000.

Nematode culture: Strains JK5810 and JK5984 were cultivated at 20°C and grown to early adulthood (24 hours after L4) in all eCLIP experiments. Developmental stage was evaluated by examining animals with a Leica Wild M3Z stereoscope for body size and stage-specific markers (e.g., vulva formation). Animals were kept on standard NGM plates and fed *E. coli* OP50 as previously described[119]. Age-synchronized first stage larvae (L1) were obtained by bleach synchronizing gravid adults by standard methods[120]. Briefly, gravid adults were treated with 2:1 bleach:4N NaOH to isolate embryos. Embryos were resuspended in M9 buffer (per 1L of buffer: 6 g Na_2HPO_4, 3 g KH_2PO_4, 5 g NaCl, 1 ml of 1 M $MgSO_4$) without food in a ventilated Erlenmeyer flask at 20°C for 20 hours. L1s were pelleted at 2500 rcf for 2 minutes, washed twice with 15 ml of M9, and distributed to 10 cm NGM plates preequilibrated to 20°C. Plates were pre-seeded with 1.5 ml of 40x concentrated OP50. Four biological replicates of each genotype were obtained. At least 100,000 animals were used per replicate, and each plate contained no more than 10,000 worms per plate.

UV crosslinking: Once animals reached L4 + 24 hour stage, live worms were quickly rinsed from plates into a 15 ml falcon tube with cold M9 + 0.01% Tween-20 (M9Tw), washed once with cold M9Tw, pelleted at 200 RCF in cold M9Tw, and transferred by glass pipet to cold, unseeded 10 cm NGM plates with minimal liquid. Animals were irradiated three times sequentially at 254 nm with 400 mJ/cm^2 in a Spectrolinker XL-1000 with the plate cover removed. Total crosslink time was approximately 5 minutes. Worms were rinsed from plates with cold M9, pelleted at 200 RCF for 1 minute, transferred to a 2 ml tube, and snap frozen in liquid nitrogen. Pellets were stored at −80°C.

Lysis and library preparation: Pellets were prepared as in iCLIP[20,121]. Pellets were thawed by adding 800 µl ice-cold iCLIP lysis buffer (50 mM Tris-HCl pH 7.4, 100 mM NaCl, 1% NP-40, 0.1% SDS, 0.5% sodium deoxycholate, protease inhibitor) and rocking for 20 minutes at 4°C. Thawed pellets were centrifuged at 1000 RCF at 4°C for 1 minute and washed three times with 800 µl cold lysis buffer. One ml of lysis buffer was added to the pellet along with a 5-mm stainless steel ball (Retsch). Lysis was performed at 4°C with a Retsch 400 MM mill mixer (3x 10 minute cycles of 30 Hz). Cracking of tube lid was prevented by adding 2 small pieces of duct tape to the lid just prior to lysis. Complete tissue lysis was confirmed by observing a small aliquot of lysate at 40x magnification. Lysate was clarified at 16,000 RCF for 15 minutes at 4°C. Protein concentration was determined using Bio-Rad Protein Assay Dye (Bio-Rad #5000006) and measuring absorbance at 595 nm on a Bio-Rad SmartSpec 3000. We used ~15 mg total protein per biological replicate in eCLIP experiments. The remainder of eCLIP was performed as outlined in SOP v1.P 20151108[58]. All IP samples used RNA adapters X1A and X1B and size-matched inputs (SMI) used adapter RiL19. See Table S6 for oligo sequences. Libraries were multiplexed with Tru-

Author Manuscript Author Manuscript Author Manuscript Author Manuscript

Seq unique-dual indices i5/i7 1-16 (https://support-docs.illumina.com/SHARE/AdapterSeq/1000000002694_17_illumina_adapter_sequences.pdf, page 41-42).

Data processing & peak calling—eCLIP data was processed as described[58]. Briefly, reads were demultiplexed and adapter sequences were trimmed using cutadapt (v. 1.18) and reads less than 18 bp were discarded. Reads mapping to repetitive *C. elegans* elements in RepBase(v. 25.08) were discarded, but all others were mapped against the *C. elegans* genome (ce10) with STAR (v. 2.7.2a). PCR duplicates were removed and peaks were normalized as previously described[58]. Peaks were called by Clipper if they were at least 2-fold enriched over input, contained at least 75 fragments per kilobase mapped (FPKM), and had a reported false discovery rate (FDR) ≤0.01. Differential peak occupancy was calculated in R(v. 3.0.2) using DiffBind(v. 3.0.15). Peaks with a log2 fold change ≥0.5 or ≤−0.5 with a significance of FDR ≤ 0.01 were called as differential. See Key Resources table for software versions and published scripts.

MEME & DAVID GO terms—Enriched motifs from each category were searched using MEME(v. 5.3.3) with the -rna - mod anr options. Tomtom(v. 5.5.2) was used to compare MEME generated motifs with known motifs. Gene ontology (GO) enrichment was done with the database for annotation, visualization, and integrated discovery website (v. DAVID 2021). Significance of GO enrichment was calculated by FDR.

Protein expression and purification—FBF-2(121-632) was previously cloned into pHMTc to create a 6xHIS:MBP:FBF-2 expression vector[34]. Site directed mutagenesis by PCR was done to introduce Y479A to create pJK2097. Transformed BL21(DE3) *E. coli* were grown at 37°C to an $A_{600\ nm}$ of 0.6 before reduction in temperature to 18°C and addition of 0.1 mM IPTG and grown for an additional 20 hours before cells were harvested by centrifugation (16,000rcf for 15 minutes at 4°C) and flash frozen for storage at −80°C. Pellets were resuspended in lysis buffer (50 mM Tris pH 8, 400 mM NaCl, 20% v/v glycerol, 0.01% Tween-20, 0.01% Triton X-100, 2 mM EDTA, 20 mM imidazole, 10 mM βME, 0.5 mg/ml lysozyme, 1x protease inhibitor and rotated at 4°C for 1 hour. Lysates were cleared by centrifugation at 16,000 rcf for 15 minutes at 4°C and filter sterilized. Lysate was applied to a HisTrap FF 5 ml column in an ÄKTA pure system preequilibrated with wash buffer (same as lysis but without lysozyme). Column was washed with 5 volumes of wash buffer before eluting and collecting fractions (same buffer as wash but with 450 mM imidazole). Fractions with most protein as determined by absorbance at 280 nm were pooled and dialyzed into 50 mM Tris pH 8, 0.5 mM EDTA, 1 mM DTT, 20% glycerol before concentration using Amicon Ultra-4 centrifugal filters (Millipore Sigma, UFC801008) and storage at −80°C.

Fluorescence polarization—A two-fold protein dilution series of proteins to be analyzed were prepared in 10 mM HEPES pH 8, 1 mM EDTA, 50 mM KCL, 1 mM DTT, 0.1 mg/ml BSA, 0.1 mg/ml yeast tRNA, 0.01% Tween-20. Proteins were incubated for 1 hour at room temperature with 0.2 nM 5’ 6-FAM RNA (synthesized by IDT) Fluorescence polarization was measured with a Synergy Hybrid H4 plate reader (BioTek). Excitation and emission wavelengths were 485 nm and 528 nm, respectively. Dissociation constants

Author Manuscript Author Manuscript Author Manuscript Author Manuscript

were estimated by non-linear regression in GraphPad Prism (9.4.1). Error bars indicate the standard deviation in three replicate measurements.

Immunostaining and imaging—Animals were staged at mid-L4 and grown for 24 hours at either 20°C or 24°C (see below) and then processed for immunostaining. For animals other than GFP reporter lines, control animals contained GFP in all somatic nuclei. This allowed us to process mutant and control animals together using somatic GFP to distinguish them. For GFP reporter strains, we compared GFP levels in experimental and control separately. To reduce variability due to GFP silencing in the *gld-1* 3'UTR reporter, these animals were grown at 24°C and were outcrossed with oma-1::GFP, a strain that licenses GFP expression[122]. While this outcross did reduce silencing, we still observed variable silencing among animals of the same strain as well as between strains. Wild-type and FBE mutant reporter hermaphrodites were staged at mid-L4 and then processed separately for immunostaining as adults 20-24 hours later.

We immunostained gonads as described[123] with minor modifications. Gonads were dissected in PBS containing 0.1% (v/v) Tween-20 (PBST) and 0.25 mM levamisole. Gonads were fixed in 4% (w/v) paraformaldehyde in PBST for 10 minutes, then permeabilized in 0.2% (v/v) Triton-X in PBST. Next, gonads were incubated for at least 30 minutes in blocking solution (0.5% (w/v) bovine serum albumin diluted in PBST or 30% goat serum in PBST (anti-FLAG)), washed 3 times with PBST, and incubated overnight at 4° with primary antibodies diluted in blocking solution. After washing, secondary antibodies were diluted in blocking solution and incubated with samples for at least 1 hour. To visualize DNA, DAPI was included with the secondary antibody at a final concentration of 1 ng/µl. After washing, samples were mounted in ProLong Gold (#P36930; Thermo Fisher Scientific) or ProLong Glass (#P36980; Thermo Fisher Scientific) and cured overnight to several days before imaging. All steps were performed at room temperature unless otherwise indicated. Antibody concentrations were as follows: αFLAG M2 (1:1000), αGFP 3E6 (1:200), αV5 (1:1000), αGLD-1 (1:200), αSP56 (1:100), αRME-2 (1:500), αPH3 (1:1000), αMouse-Alexa647 (1:1000), αRabbit-Alexa488 (1:1000). See Key Resources table for antibody information. Imaging was performed on a Leica SP8 confocal microscope.

Single molecule fluorescence in situ hybridization (smFISH)—Single molecule fluorescence *in situ* hybridization (smFISH) was performed as described previously[124] with published *lst-1* exon probes[46] labeled with CAL Fluor Red 610® (0.25 µM). Animals 24 h after mid-L4, were dissected in 100 µl PBS, 0.1% Tween-20 (PBST) containing 0.1% levamisole. Dissected worms were pelleted at 1500 rpm for 30 seconds, fixed in 1 ml PBST, 3.7% formaldehyde, pelleted, washed in PBST, and permeabilized in PBS containing 0.1% Triton X-100 for 10 min at room temperature. Samples were washed two times in PBST, resuspended in 1 ml 70% ethanol and stored at 4°C. Gonads were pelleted, incubated with 1 ml smFISH wash buffer (2x SSC, 10% formamide, 0.1% Tween-20) for 5 minutes at room temperature, pelleted and resuspended in hybridization buffer (228 mM Dextran sulfate, 2X SSC, 10% deionized formamide in nuclease-free water) containing 0.25 µM *lst-1* exon probe labeled with CAL Fluor Red 610® (Biosearch Technologies). Samples were hybridized overnight at 37°C, protected from light. Following hybridization, samples were

Author Manuscript Author Manuscript Author Manuscript Author Manuscript

washed smFISH wash buffer (2x SSC, 10% deionized formamide in nuclease-free water, 0.1% Tween-20) at room temperature, incubated with 1 ml wash buffer containing 1 μg/ml DAPI for 30 min, washed two additional times, and then mounted in ProLong Gold (Life Technologies Corporation, Carlsbad, CA) and allowed to cure overnight to several days before imaging. Images were acquired using a Leica SP8 confocal microscope.

Co-immunoprecipitation—Worm lysates were prepared as above for eCLIP without UV crosslinking in coIP buffer (20 mM Tris pH 8, 150 mM NaCl, 2 mM EDTA, 5 mM $MgCl_2$, 1% Triton-X). To prepare antibody conjugated beads, 10 μg mouse αFLAG was incubated with 4.5 mg protein G Dynabeads (Novex, Life Technologies, #10003D) for 60 minutes at RT. Beads were then washed 2x with coIP buffer. 20 mg of total protein was incubated with the antibody-bead mixture for 4 hours at 4°C, with the presence of 250U/mL benzonase nuclease. Beads were washed three times with coIP buffer, and then three times with wash buffer (same as coIP but with 500 mM NaCl). Samples then were eluted (2% (w/v) SDS, 0.1% βME, 10% glycerol, 50 mM Tris pH 8) for 10 minutes at 100°C and analyzed by SDS-PAGE (4-20% acrylamide gel). Three independent replicates were performed for each coIP, with a representative blot shown. Antibody concentrations were as follows: αFLAG (1:1000), αV5 (1:1000), αGAPDH (1:10,000), αActin (1:40,000), αMouse-HRP (1:10,000). See Key Resources table for antibody information.

Phenotypic analysis—Adult animals were scored as fertile or sterile using a dissecting scope. Sterile animals were then mounted on agarose pads and scored for germ cell phenotypes on a compound microscope. Progenitor zone length in germ cell diameters (gcd) was scored in DAPI-stained animals by counting germ cell diameters from the distal tip of the germline to the start of meiotic entry[12].

QUANTIFICATION AND STATISTICAL ANALYSIS

Protein levels were quantitated in summed projections of confocal stacks using ImageJ as described[125]. Briefly, a line (linewidth = 50 pixels or 30 pixels) was drawn along the distal-proximal axis of the germline. Pixel intensity was measured using the plot profile function. Intensities were copied into Excel. Data was then copied into Graphpad Prism 9.4.1 and the Row Statistics function was used to calculate mean values along the distal-proximal axis. We normalized the means of both wild-type and mutants to the maximum level of protein found in the distal 100 microns of wild-type germlines. The normalized means were then graphed with 95% confidence intervals. Replicates and n for each experiment given in figure legends. P-values were calculated in Graphpad Prism 9.3.1 or 10.0.3 using an unpaired t-test assuming equal variance. P-values are given for pooled data from regions of the germline indicated in each graph. Significance: *** $p < 0.001$, ** $p < 0.01$, * $p < 0.05$, ns (not significant) $p > 0.05$.

Supplementary Material

Refer to Web version on PubMed Central for supplementary material.

Author Manuscript Author Manuscript Author Manuscript Author Manuscript

Acknowledgements

The authors thank members of the Kimble and Wickens labs for insightful discussions throughout the course of this work. We thank Jane Selegue, Jadwiga Forster, Kyle Krueger, Hezouwe Walada, Deep Kapadia, Garrett Gunderson, and Tim Guthrie for assistance and the Michael Sheets lab for use of equipment. We thank Traci Hall and Chen Qiu for comments on the manuscript and Laura Vanderploeg for help with figure preparation. Some strains were provided by the CGC, which is funded by NIH Office of Research Infrastructure Programs (P40 OD010440). This work was supported by the National Science Foundation Graduate Research Fellowship Program under Grant Nos. DGE-1256259 and DGE-1747503 to BHC; NIH R01 GM50942 to MW; and NIH R01 GM134119 to JK. Any opinions, findings, and conclusions or recommendations expressed in this material and those of the authors and do not necessarily reflect the views of the National Science Foundation.

References

1. Keene JD (2007). RNA regulons: coordination of post-transcriptional events. Nature Reviews Genetics 8, 533–543. 10.1038/nrg2111.
2. Ule J, and Darnell RB (2006). RNA binding proteins and the regulation of neuronal synaptic plasticity. Current Opinion in Neurobiology 16, 102–110. 10.1016/j.conb.2006.01.003. [PubMed: 16418001]
3. Lapointe CP, Wilinski D, Saunders HAJ, and Wickens M (2015). Protein-RNA networks revealed through covalent RNA marks. Nature Methods 12, 1163–1170. 10.1038/nmeth.3651. [PubMed: 26524240]
4. Hentze MW, Castello A, Schwarzl T, and Preiss T (2018). A brave new world of RNA-binding proteins. Nat Rev Mol Cell Biol 19, 327–341. 10.1038/nrm.2017.130. [PubMed: 29339797]
5. Singh G, Pratt G, Yeo GW, and Moore MJ (2015). The Clothes Make the mRNA: Past and Present Trends in mRNP Fashion. Annual Review of Biochemistry 84, 325–354. 10.1146/annurev-biochem-080111-092106.
6. Corley M, Burns MC, and Yeo GW (2020). How RNA-Binding Proteins Interact with RNA: Molecules and Mechanisms. Mol Cell 78, 9–29. 10.1016/j.molcel.2020.03.011. [PubMed: 32243832]
7. Gebauer F, Schwarzl T, Valcárcel J, and Hentze MW (2021). RNA-binding proteins in human genetic disease. Nat Rev Genet 22, 185–198. 10.1038/s41576-020-00302-y. [PubMed: 33235359]
8. Albarqi MMY, and Ryder SP (2022). The role of RNA-binding proteins in orchestrating germline development in Caenorhabditis elegans. Front Cell Dev Biol 10, 1094295. 10.3389/fcell.2022.1094295. [PubMed: 36684428]
9. Goldstrohm AC, Hall TMT, and McKenney KM (2018). Post-transcriptional Regulatory Functions of Mammalian Pumilio Proteins. Trends Genet 34, 972–990. 10.1016/j.tig.2018.09.006. [PubMed: 30316580]
10. Miller MA, and Olivas WM (2011). Roles of Puf proteins in mRNA degradation and translation. Wiley Interdiscip Rev RNA 2, 471–492. 10.1002/wrna.69. [PubMed: 21957038]
11. Uyhazi KE, Yang Y, Liu N, Qi H, Huang XA, Mak W, Weatherbee SD, de Prisco N, Gennarino VA, Song X, and Lin H (2020). Pumilio proteins utilize distinct regulatory mechanisms to achieve complementary functions required for pluripotency and embryogenesis. Proc Natl Acad Sci U S A 117, 7851–7862. 10.1073/pnas.1916471117. [PubMed: 32198202]
12. Gennarino VA, Palmer EE, McDonell LM, Wang L, Adamski CJ, Koire A, See L, Chen CA, Schaaf CP, Rosenfeld JA, et al. (2018). A Mild PUM1 Mutation Is Associated with Adult-Onset Ataxia, whereas Haploinsufficiency Causes Developmental Delay and Seizures. Cell 172, 924–936.e911. 10.1016/j.cell.2018.02.006. [PubMed: 29474920]
13. Naudin C, Hattabi A, Michelet F, Miri-Nezhad A, Benyoucef A, Pflumio F, Guillonneau F, Fichelson S, Vigon I, Dusanter-Fourt I, and Lauret E (2017). PUMILIO/FOXP1 signaling drives expansion of hematopoietic stem/progenitor and leukemia cells. Blood 129, 2493–2506. 10.1182/blood-2016-10-747436. [PubMed: 28232582]
14. Botta S, de Prisco N, Chemiakine A, Brandt V, Cabaj M, Patel P, Doron-Mandel E, Treadway CJ, Jovanovic M, Brown NG, et al. (2023). Dosage sensitivity to Pumilio1 variants in the mouse brain reflects distinct molecular mechanisms. Embo j, e112721. 10.15252/embj.2022112721. [PubMed: 37070548]

Author Manuscript Author Manuscript Author Manuscript Author Manuscript

15. Wickens M, Bernstein DS, Kimble J, and Parker R (2002). A PUF family portrait: 3'UTR regulation as a way of life. Trends in Genetics 18, 150–157. [PubMed: 11858839]
16. Olivas W, and Parker R (2000). The Puf3 protein is a transcript-specific regulator of mRNA degradation in yeast. Embo j 19, 6602–6611. 10.1093/emboj/19.23.6602. [PubMed: 11101532]
17. Kershner AM, and Kimble J (2010). Genome-wide analysis of mRNA targets for Caenorhabditis elegans FBF, a conserved stem cell regulator. Proceedings of the National Academy of Sciences 107, 3936–3941. 10.1073/pnas.1000495107.
18. Merritt C, and Seydoux G (2010). The Puf RNA-binding proteins FBF-1 and FBF-2 inhibit the expression of synaptonemal complex proteins in germline stem cells. Development 137, 1787–1798. 10.1242/dev.050799. [PubMed: 20431119]
19. Porter DF, Prasad A, Carrick BH, Kroll-Connor P, Wickens M, and Kimble J (2019). Toward Identifying Subnetworks from FBF Binding Landscapes in Caenorhabditis Spermatogenic or Oogenic Germlines. G3 (Bethesda) 9, 153–165. 10.1534/g3.118.200300. [PubMed: 30459181]
20. Prasad A, Porter DF, Kroll-Conner PL, Mohanty I, Ryan AR, Crittenden SL, Wickens M, and Kimble J (2016). The PUF binding landscape in metazoan germ cells. Rna 22, 1026–1043. 10.1261/rna.055871.116. [PubMed: 27165521]
21. Gerber AP, Herschlag D, and Brown PO (2004). Extensive association of functionally and cytotopically related mRNAs with Puf family RNA-binding proteins in yeast. PLoS Biol 2, E79. 10.1371/journal.pbio.0020079. [PubMed: 15024427]
22. Lapointe CP, Preston MA, Wilinski D, Saunders HAJ, Campbell ZT, and Wickens M (2017). Architecture and dynamics of overlapped RNA regulatory networks. Rna 23, 1636–1647. 10.1261/rna.062687.117. [PubMed: 28768715]
23. Crittenden SL, Bernstein DS, Bachorik JL, Thompson BE, Gallegos M, Petcherski AG, Moulder G, Barstead R, Wickens M, and Kimble J (2002). A conserved RNA-binding protein controls germline stem cells in Caenorhabditis elegans. Nature 417, 660–663. 10.1038/nature754. [PubMed: 12050669]
24. Zhang B, Gallegos M, Puoti A, Durkin E, Fields S, Kimble J, and Wickens MP (1997). A conserved RNA-binding protein that regulates sexual fates in the C. elegans hermaphrodite germ line. Nature 390, 477–484. 10.1038/37297. [PubMed: 9393998]
25. Campbell Zachary T., Bhimsaria D, Valley Cary T., Rodriguez-Martinez Jose A., Menichelli E, Williamson James R., Ansari AZ, and Wickens M (2012). Cooperativity in RNA-Protein Interactions: Global Analysis of RNA Binding Specificity. Cell Reports 1, 570–581. 10.1016/j.celrep.2012.04.003. [PubMed: 22708079]
26. Campbell ZT, Menichelli E, Friend K, Wu J, Kimble J, Williamson JR, and Wickens M (2012). Identification of a Conserved Interface between PUF and CPEB Proteins. Journal of Biological Chemistry 287, 18854–18862. 10.1074/jbc.m112.352815. [PubMed: 22496444]
27. Van Etten J, Schagat TL, Hrit J, Weidmann CA, Brumbaugh J, Coon JJ, and Goldstrohm AC (2012). Human Pumilio Proteins Recruit Multiple Deadenylases to Efficiently Repress Messenger RNAs. Journal of Biological Chemistry 287, 36370–36383. 10.1074/jbc.m112.373522. [PubMed: 22955276]
28. Goldstrohm AC, Hook BA, Seay DJ, and Wickens M (2006). PUF proteins bind Pop2p to regulate messenger mRNAs. Nature Structural & Molecular Biology 13, 533–539.
29. Goldstrohm AC, Seay DJ, Hook BA, and Wickens M (2006). PUF Protein-mediated Deadenylation Is Catalyzed by Ccr4p. Journal of Biological Chemistry 282, 109–114. 10.1074/jbc.m609413200. [PubMed: 17090538]
30. Arvola RM, Weidmann CA, Tanaka Hall TM, and Goldstrohm AC (2017). Combinatorial control of messenger RNAs by Pumilio, Nanos and Brain Tumor Proteins. RNA Biol 14, 1445–1456. 10.1080/15476286.2017.1306168. [PubMed: 28318367]
31. Ferdous AS, Costa Dos Santos SJ, Kanzler CR, Shin H, Carrick BH, Crittenden SL, Wickens M, and Kimble J (2023). The in vivo functional significance of PUF hub partnerships in C. elegans germline stem cells. Development. 10.1242/dev.201705.
32. Qiu C, Bhat VD, Rajeev S, Zhang C, Lasley AE, Wine RN, Campbell ZT, and Hall TMT (2019). A crystal structure of a collaborative RNA regulatory complex reveals mechanisms to refine target specificity. Elife 8. 10.7554/eLife.48968.

Author Manuscript Author Manuscript Author Manuscript Author Manuscript

33. Hafner M, Landthaler M, Burger L, Khorshid M, Hausser J, Berninger P, Rothballer A, Ascano M, Jungkamp A-C, Munschauer M, et al. (2010). Transcriptome-wide Identification of RNA-Binding Protein and MicroRNA Target Sites by PAR-CLIP. Cell 141, 129–141. 10.1016/j.cell.2010.03.009. [PubMed: 20371350]
34. Bernstein D, Hook B, Hajarnavis A, Opperman L, and Wickens M (2005). Binding specificity and mRNA targets of a C. elegans PUF protein, FBF-1. Rna 11, 447–458. 10.1261/rna.7255805. [PubMed: 15769874]
35. Opperman L, Hook B, DeFino M, Bernstein DS, and Wickens M (2005). A single spacer nucleotide determines the specificities of two mRNA regulatory proteins. Nature Structural & Molecular Biology 12, 945–951. 10.1038/nsmb1010.
36. Wang Y, Opperman L, Wickens M, and Hall TM (2009). Structural basis for specific recognition of multiple mRNA targets by a PUF regulatory protein. Proc Natl Acad Sci U S A 106, 20186–20191. 10.1073/pnas.0812076106. [PubMed: 19901328]
37. Zanetti S, Grinschgl S, Meola M, Belfiore M, Rey S, Bianchi P, and Puoti A (2012). The sperm-oocyte switch in the C. elegans hermaphrodite is controlled through steady-state levels of the fem-3 mRNA. Rna 18, 1385–1394. 10.1261/rna.031237.111. [PubMed: 22635404]
38. Shin H, Haupt KA, Kershner AM, Kroll-Conner P, Wickens M, and Kimble J (2017). SYGL-1 and LST-1 link niche signaling to PUF RNA repression for stem cell maintenance in Caenorhabditis elegans. PLoS Genet 13, e1007121. 10.1371/journal.pgen.1007121. [PubMed: 29232700]
39. Kaye JA, Rose NC, Goldsworthy B, Goga A, and L'Etoile ND (2009). A 3'UTR Pumilio-binding element directs translational activation in olfactory sensory neurons. Neuron 61, 57–70. 10.1016/j.neuron.2008.11.012. [PubMed: 19146813]
40. Suh N, Crittenden SL, Goldstrohm A, Hook B, Thompson B, Wickens M, and Kimble J (2009). FBF and Its Dual Control of gld-1 Expression in the Caenorhabditis elegans Germline. Genetics 181, 1249–1260. 10.1534/genetics.108.099440. [PubMed: 19221201]
41. Edwards TA, Pyle SE, Wharton RP, and Aggarwal AK (2001). Structure of Pumilio Reveals Similarity between RNA and Peptide Binding Motifs. Cell 105, 281–289. 10.1016/s0092-8674(01)00318-x. [PubMed: 11336677]
42. Wang X, Zamore PD, and Hall TMT (2001). Crystal Structure of a Pumilio Homology Domain. Molecular Cell 7, 855–865. 10.1016/s1097-2765(01)00229-5. [PubMed: 11336708]
43. Wu J, Campbell ZT, Menichelli E, Wickens M, and Williamson JR (2013). A protein • protein interaction platform involved in recruitment of GLD-3 to the FBF • fem-3 mRNA complex. J Mol Biol 425, 738–754. 10.1016/j.jmb.2012.11.013. [PubMed: 23159559]
44. Qiu C, Zhang Z, Wine RN, Campbell ZT, Zhang J, and Hall TMT (2023). Intra- and inter-molecular regulation by intrinsically-disordered regions governs PUF protein RNA binding. Nat Commun 14, 7323. 10.1038/s41467-023-43098-1. [PubMed: 37953271]
45. Kershner AM, Shin H, Hansen TJ, and Kimble J (2014). Discovery of two GLP-1/Notch target genes that account for the role of GLP-1/Notch signaling in stem cell maintenance. Proceedings of the National Academy of Sciences 111, 3739–3744. 10.1073/pnas.1401861111.
46. Haupt KA, Enright AL, Ferdous AS, Kershner AM, Shin H, Wickens M, and Kimble J (2019). The molecular basis of LST-1 self-renewal activity and its control of stem cell pool size. Development 146. 10.1242/dev.181644.
47. Eckmann CR, Kraemer B, Wickens M, and Kimble J (2002). GLD-3, a Bicaudal-C homolog that inhibits FBF to control germline sex determination in *C. elegans*. Developmental Cell 3, 697–710. [PubMed: 12431376]
48. Luitjens C, Gallegos M, Kraemer B, Kimble J, and Wickens M (2000). CPEB proteins control two key steps in spermatogenesis in C. elegans. Genes Dev 14, 2596–2609. 10.1101/gad.831700. [PubMed: 11040214]
49. Wang X, Olson JR, Rasoloson D, Ellenbecker M, Bailey J, and Voronina E (2016). Dynein light chain DLC-1 promotes localization and function of the PUF protein FBF-2 in germline progenitor cells. Development 143, 4643–4653. 10.1242/dev.140921. [PubMed: 27864381]
50. Weidmann CA, Qiu C, Arvola RM, Lou TF, Killingsworth J, Campbell ZT, Tanaka Hall TM, and Goldstrohm AC (2016). Drosophila Nanos acts as a molecular clamp that modulates the RNA-binding and repression activities of Pumilio. Elife 5. 10.7554/eLife.17096.

Author Manuscript Author Manuscript Author Manuscript Author Manuscript

51. Menichelli E, Wu J, Campbell ZT, Wickens M, and Williamson JR (2013). Biochemical characterization of the *Caenorhabditis elegans* FBF • CPB-1 translational regulation complex identifies conserved protein interaction hotspots. J Mol Biol 425, 725–737. 10.1016/j.jmb.2012.11.012. [PubMed: 23159558]
52. Friend K, Campbell ZT, Cooke A, Kroll-Conner P, Wickens MP, and Kimble J (2012). A conserved PUF–Ago–eEF1A complex attenuates translation elongation. Nature Structural & Molecular Biology 19, 176–183. 10.1038/nsmb.2214.
53. Arvola RM, Chang CT, Buytendorp JP, Levdansky Y, Valkov E, Freddolino PL, and Goldstrohm AC (2020). Unique repression domains of Pumilio utilize deadenylation and decapping factors to accelerate destruction of target mRNAs. Nucleic Acids Res 48, 1843–1871. 10.1093/nar/gkz1187. [PubMed: 31863588]
54. Enwerem III, Elrod ND, Chang CT, Lin A, Ji P, Bohn JA, Levdansky Y, Wagner EJ, Valkov E, and Goldstrohm AC (2021). Human Pumilio proteins directly bind the CCR4-NOT deadenylase complex to regulate the transcriptome. Rna 27, 445–464. 10.1261/rna.078436.120. [PubMed: 33397688]
55. Webster MW, Stowell JA, and Passmore LA (2019). RNA-binding proteins distinguish between similar sequence motifs to promote targeted deadenylation by Ccr4-Not. Elife 8. 10.7554/eLife.40670.
56. Lamont LB, Crittenden SL, Bernstein D, Wickens M, and Kimble J (2004). FBF-1 and FBF-2 regulate the size of the mitotic region in the C. elegans germline. Dev Cell 7, 697–707. 10.1016/j.devcel.2004.09.013. [PubMed: 15525531]
57. Qiu C, Wine RN, Campbell ZT, and Hall TMT (2022). Bipartite interaction sites differentially modulate RNA-binding affinity of a protein complex essential for germline stem cell self-renewal. Nucleic Acids Res 50, 536–548. 10.1093/nar/gkab1220. [PubMed: 34908132]
58. Van Nostrand EL, Pratt GA, Shishkin AA, Gelboin-Burkhart C, Fang MY, Sundararaman B, Blue SM, Nguyen TB, Surka C, Elkins K, et al. (2016). Robust transcriptome-wide discovery of RNA-binding protein binding sites with enhanced CLIP (eCLIP). Nature Methods 13, 508–514. 10.1038/nmeth.3810. [PubMed: 27018577]
59. Jarmoskaite I, Denny SK, Vaidyanathan PP, Becker WR, Andreasson JOL, Layton CJ, Kappel K, Shivashankar V, Sreenivasan R, Das R, et al. (2019). A Quantitative and Predictive Model for RNA Binding by Human Pumilio Proteins. Mol Cell 74, 966–981.e918. 10.1016/j.molcel.2019.04.012. [PubMed: 31078383]
60. Stark R, and Brown GD DiffBind: differential binding analysis of ChIP-seq peak data. Bioconductor http://bioconductor.org/packages/release/bioc/html/DiffBind.html.
61. Wang X, Ellenbecker M, Hickey B, Day NJ, Osterli E, Terzo M, and Voronina E (2020). Antagonistic control of Caenorhabditis elegans germline stem cell proliferation and differentiation by PUF proteins FBF-1 and FBF-2. Elife 9. 10.7554/eLife.52788.
62. Voronina E, Paix A, and Seydoux G (2012). The P granule component PGL-1 promotes the localization and silencing activity of the PUF protein FBF-2 in germline stem cells. Development 139, 3732–3740. 10.1242/dev.083980. [PubMed: 22991439]
63. Coller JM, Gray NK, and Wickens MP (1998). mRNA stabilization by poly(A) binding protein is independent of poly(A) and requires translation. Genes & Development 12, 3226–3235. 10.1101/gad.12.20.3226. [PubMed: 9784497]
64. De Gregorio E, Preiss T, and Hentze MW (1999). Translation driven by an eIF4G core domain in vivo. Embo j 18, 4865–4874. 10.1093/emboj/18.17.4865. [PubMed: 10469664]
65. Aoki ST, Porter DF, Prasad A, Wickens M, Bingman CA, and Kimble J (2018). An RNA-Binding Multimer Specifies Nematode Sperm Fate. Cell Rep 23, 3769–3775. 10.1016/j.celrep.2018.05.095. [PubMed: 29949762]
66. Brenner JL, and Schedl T (2016). Germline Stem Cell Differentiation Entails Regional Control of Cell Fate Regulator GLD-1 in Caenorhabditis elegans. Genetics 202, 1085–1103. 10.1534/genetics.115.185678. [PubMed: 26757772]
67. Francis R, Barton MK, Kimble J, and Schedl T (1995). gld-1, a tumor suppressor gene required for oocyte development in Caenorhabditis elegans. Genetics 139, 579–606. 10.1093/genetics/139.2.579. [PubMed: 7713419]

Author Manuscript Author Manuscript Author Manuscript Author Manuscript

68. Francis R, Maine E, and Schedl T (1995). Analysis of the multiple roles of gld-1 in germline development: interactions with the sex determination cascade and the glp-1 signaling pathway. Genetics 139, 607–630. 10.1093/genetics/139.2.607. [PubMed: 7713420]
69. Jones AR, Francis R, and Schedl T (1996). GLD-1, a cytoplasmic protein essential for oocyte differentiation, shows stage- and sex-specific expression during Caenorhabditis elegans germline development. Dev Biol 180, 165–183. 10.1006/dbio.1996.0293. [PubMed: 8948583]
70. Theil K, Imami K, and Rajewsky N (2019). Identification of proteins and miRNAs that specifically bind an mRNA in vivo. Nat Commun 10, 4205. 10.1038/s41467-019-12050-7. [PubMed: 31527589]
71. Tollervey JR, Curk T, Rogelj B, Briese M, Cereda M, Kayikci M, König J, Hortobágyi T, Nishimura AL, Zupunski V, et al. (2011). Characterizing the RNA targets and position-dependent splicing regulation by TDP-43. Nat Neurosci 14, 452–458. 10.1038/nn.2778. [PubMed: 21358640]
72. Hallegger M, Chakrabarti AM, Lee FCY, Lee BL, Amalietti AG, Odeh HM, Copley KE, Rubien JD, Portz B, Kuret K, et al. (2021). TDP-43 condensation properties specify its RNA-binding and regulatory repertoire. Cell 184, 4680–4696.e4622. 10.1016/j.cell.2021.07.018. [PubMed: 34380047]
73. Porter DF, Miao W, Yang X, Goda GA, Ji AL, Donohue LKH, Aleman MM, Dominguez D, and Khavari PA (2021). easyCLIP analysis of RNA-protein interactions incorporating absolute quantification. Nat Commun 12, 1569. 10.1038/s41467-021-21623-4. [PubMed: 33692367]
74. Porter DF, Koh YY, VanVeller B, Raines RT, and Wickens M (2015). Target selection by natural and redesigned PUF proteins. Proceedings of the National Academy of Sciences 112, 15868–15873. 10.1073/pnas.1508501112.
75. Jankowsky E, and Harris ME (2015). Specificity and nonspecificity in RNA-protein interactions. Nature reviews. Molecular cell biology 16, 533–544. 10.1038/nrm4032. [PubMed: 26285679]
76. Wharton RP, and Struhl G (1991). RNA regulatory elements mediate control of Drosophila body pattern by the posterior morphogen nanos. Cell 67, 955–967. 10.1016/0092-8674(91)90368-9. [PubMed: 1720354]
77. Wreden C, Verrotti AC, Schisa JA, Lieberfarb ME, and Strickland S (1997). Nanos and pumilio establish embryonic polarity in Drosophila by promoting posterior deadenylation of hunchback mRNA. Development 124, 3015–3023. 10.1242/dev.124.15.3015. [PubMed: 9247343]
78. Lee C-D, and Tu Benjamin P. (2015). Glucose-Regulated Phosphorylation of the PUF Protein Puf3 Regulates the Translational Fate of Its Bound mRNAs and Association with RNA Granules. Cell Reports 11, 1638–1650. 10.1016/j.celrep.2015.05.014. [PubMed: 26051939]
79. Yang CR, Rajkovic G, Daldello EM, Luong XG, Chen J, and Conti M (2020). The RNA-binding protein DAZL functions as repressor and activator of mRNA translation during oocyte maturation. Nat Commun 11, 1399. 10.1038/s41467-020-15209-9. [PubMed: 32170089]
80. Liu B, Li Y, Stackpole EE, Novak A, Gao Y, Zhao Y, Zhao X, and Richter JD (2018). Regulatory discrimination of mRNAs by FMRP controls mouse adult neural stem cell differentiation. Proc Natl Acad Sci U S A 115, E11397–e11405. 10.1073/pnas.1809588115. [PubMed: 30373821]
81. Ahringer J, and Kimble J (1991). Control of the sperm-oocyte switch in *Caenorhabditis elegans hermaphrodites by the fem-3* 3′ untranslated region. Nature 349, 346–348. [PubMed: 1702880]
82. Mangio RS, Votra S, and Pruyne D (2015). The canonical eIF4E isoform of C. elegans regulates growth, embryogenesis, and germline sex-determination. Biol Open 4, 843–851. 10.1242/bio.011585. [PubMed: 25979704]
83. Kalchhauser I, Farley BM, Pauli S, Ryder SP, and Ciosk R (2011). FBF represses the Cip/Kip cell-cycle inhibitor CKI-2 to promote self-renewal of germline stem cells in C. elegans. Embo j 30, 3823–3829. 10.1038/emboj.2011.263. [PubMed: 21822213]
84. Fox PM, Vought VE, Hanazawa M, Lee MH, Maine EM, and Schedl T (2011). Cyclin E and CDK-2 regulate proliferative cell fate and cell cycle progression in the *C. elegans* germline. Development 138, 2223–2234. 10.1242/dev.059535. [PubMed: 21558371]
85. Jeong J, Verheyden JM, and Kimble J (2011). Cyclin E and Cdk2 control GLD-1, the mitosis/meiosis decision, and germline stem cells in *Caenorhabditis elegans*. PLoS Genetics 7, e1001348. 10.1371/journal.pgen.1001348. [PubMed: 21455289]

Author Manuscript Author Manuscript Author Manuscript Author Manuscript

86. Choi PS, and Thomas-Tikhonenko A (2021). RNA-binding proteins of COSMIC importance in cancer. J Clin Invest 131. 10.1172/jci151627.
87. Kapeli K, Martinez FJ, and Yeo GW (2017). Genetic mutations in RNA-binding proteins and their roles in ALS. Hum Genet 136, 1193–1214. 10.1007/s00439-017-1830-7. [PubMed: 28762175]
88. Prashad S, and Gopal PP (2021). RNA-binding proteins in neurological development and disease. RNA Biol 18, 972–987. 10.1080/15476286.2020.1809186. [PubMed: 32865115]
89. Qin H, Ni H, Liu Y, Yuan Y, Xi T, Li X, and Zheng L (2020). RNA-binding proteins in tumor progression. J Hematol Oncol 13, 90. 10.1186/s13045-020-00927-w. [PubMed: 32653017]
90. Gennarino Vincenzo A., Singh Ravi K., White Joshua J., De Maio A, Han K, Kim J-Y, Jafar-Nejad P, di Ronza A, Kang H, Sayegh Layal S., et al. (2015). Pumilio1 Haploinsufficiency Leads to SCA1-like Neurodegeneration by Increasing Wild-Type Ataxin1 Levels. Cell 160, 1087–1098. 10.1016/j.cell.2015.02.012. [PubMed: 25768905]
91. Aoki ST, Crittenden SL, Lynch TR, Bingman CA, Wickens M, and Kimble J (2018). Nematode germ granule assembly is linked to mRNA repression. bioRxiv. 10.1101/382838.
92. Jan E, Motzny CK, Graves LE, and Goodwin EB (1999). The STAR protein, GLD-1, is a translational regulator of sexual identity in Caenorhabditis elegans. Embo j 18, 258–269. 10.1093/emboj/18.1.258. [PubMed: 9878068]
93. Ward S, Roberts TM, Strome S, Pavalko FM, and Hogan E (1986). Monoclonal antibodies that recognize a polypeptide antigenic determinant shared by multiple Caenorhabditis elegans sperm-specific proteins. J Cell Biol 102, 1778–1786. 10.1083/jcb.102.5.1778. [PubMed: 2422180]
94. Grant B, and Hirsh D (1999). Receptor-mediated endocytosis in the Caenorhabditis elegans oocyte. Mol Biol Cell 10, 4311–4326. 10.1091/mbc.10.12.4311. [PubMed: 10588660]
95. Brenner S (1974). The genetics of Caenorhabditis elegans. Genetics 77, 71–94. 10.1093/genetics/77.1.71. [PubMed: 4366476]
96. Frøkjær-Jensen C, Davis MW, Sarov M, Taylor J, Flibotte S, LaBella M, Pozniakovsky A, Moerman DG, and Jorgensen EM (2014). Random and targeted transgene insertion in Caenorhabditis elegans using a modified Mos1 transposon. Nat Methods 11, 529–534. 10.1038/nmeth.2889. [PubMed: 24820376]
97. Ellis RE, and Kimble J (1995). The *fog-3* gene and regulation of cell fate in the germ line of *Caenorhabditis elegans*. Genetics 139, 561–577. [PubMed: 7713418]
98. Martin M (2011). Cutadapt removes adapter sequences from high-throughput sequencing reads. 2011 17, 3 %J EMBnet.journal. 10.14806/ej.17.1.200.
99. Dobin A, Davis CA, Schlesinger F, Drenkow J, Zaleski C, Jha S, Batut P, Chaisson M, and Gingeras TR (2013). STAR: ultrafast universal RNA-seq aligner. Bioinformatics 29, 15–21. 10.1093/bioinformatics/bts635. [PubMed: 23104886]
100. Li H, Handsaker B, Wysoker A, Fennell T, Ruan J, Homer N, Marth G, Abecasis G, and Durbin R (2009). The Sequence Alignment/Map format and SAMtools. Bioinformatics 25, 2078–2079. 10.1093/bioinformatics/btp352. [PubMed: 19505943]
101. Quinlan AR, and Hall IM (2010). BEDTools: a flexible suite of utilities for comparing genomic features. Bioinformatics 26, 841–842. 10.1093/bioinformatics/btq033. [PubMed: 20110278]
102. Bailey TL, and Elkan C (1994). Fitting a mixture model by expectation maximization to discover motifs in biopolymers. Proc Int Conf Intell Syst Mol Biol 2, 28–36. [PubMed: 7584402]
103. Gupta S, Stamatoyannopoulos JA, Bailey TL, and Noble WS (2007). Quantifying similarity between motifs. Genome Biology 8, R24. 10.1186/gb-2007-8-2-r24. [PubMed: 17324271]
104. Van Rossum G, and Drake FL Jr (1995). Python reference manual. Centrum voor Wiskunde en Informatica Amsterdam.
105. Anders S, Pyl PT, and Huber W (2015). HTSeq--a Python framework to work with high-throughput sequencing data. Bioinformatics 31, 166–169. 10.1093/bioinformatics/btu638. [PubMed: 25260700]
106. Pedregosa F, Varoquaux G, Gramfort A, Michel V, Thirion B, Grisel O, Blondel M, Prettenhofer P, Weiss R, Dubourg V, et al. (2011). Scikit-learn: Machine Learning in Python. Journal of Machine Learning Research 12, 2825–2830.
107. Virtanen P, Gommers R, Oliphant TE, Haberland M, Reddy T, Cournapeau D, Burovski E, Peterson P, Weckesser W, Bright J, et al. (2020). SciPy 1.0: fundamental algorithms

Author Manuscript Author Manuscript Author Manuscript Author Manuscript

for scientific computing in Python. Nat Methods 17, 261–272. 10.1038/s41592-019-0686-2. [PubMed: 32015543]

108. Hunter JD (2007). Matplotlib: A 2D Graphics Environment. Computing in Science & Engineering 9, 90–95. 10.1109/MCSE.2007.55.
109. Waskom ML (2021). seaborn: statistical data visualization. Journal of Open Source Software 6 (60), 3021. 10.21105/joss.03021.
110. Yu G, Wang LG, and He QY (2015). ChIPseeker: an R/Bioconductor package for ChIP peak annotation, comparison and visualization. Bioinformatics 31, 2382–2383. 10.1093/bioinformatics/btv145. [PubMed: 25765347]
111. Lawrence M, Huber W, Pagès H, Aboyoun P, Carlson M, Gentleman R, Morgan MT, and Carey VJ (2013). Software for computing and annotating genomic ranges. PLoS Comput Biol 9, e1003118. 10.1371/journal.pcbi.1003118. [PubMed: 23950696]
112. Wall L, Christiansen T, and Orwant J (2000). Programming perl. O'Reilly Media, Inc.
113. Arribere JA, Bell RT, Fu BX, Artiles KL, Hartman PS, and Fire AZ (2014). Efficient marker-free recovery of custom genetic modifications with CRISPR/Cas9 in Caenorhabditis elegans. Genetics 198, 837–846. 10.1534/genetics.114.169730. [PubMed: 25161212]
114. Dokshin GA, Ghanta KS, Piscopo KM, and Mello CC (2018). Robust Genome Editing with Short Single-Stranded and Long, Partially Single-Stranded DNA Donors in Caenorhabditis elegans. Genetics 210, 781–787. 10.1534/genetics.118.301532. [PubMed: 30213854]
115. Paix A, Folkmann A, Rasoloson D, and Seydoux G (2015). High Efficiency, Homology-Directed Genome Editing in Caenorhabditis elegans Using CRISPR-Cas9 Ribonucleoprotein Complexes. Genetics 201, 47–54. 10.1534/genetics.115.179382. [PubMed: 26187122]
116. Frokjaer-Jensen C, Davis MW, Hopkins CE, Newman BJ, Thummel JM, Olesen SP, Grunnet M, and Jorgensen EM (2008). Single-copy insertion of transgenes in Caenorhabditis elegans. Nat Genet 40, 1375–1383. 10.1038/ng.248. [PubMed: 18953339]
117. Mirdita M, Schütze K, Moriwaki Y, Heo L, Ovchinnikov S, and Steinegger M (2022). ColabFold: making protein folding accessible to all. Nat Methods 19, 679–682. 10.1038/s41592-022-01488-1. [PubMed: 35637307]
118. Evans R, O'Neill M, Pritzel A, Antropova N, Senior A, Green T, Žídek A, Bates R, Blackwell S, Yim J, et al. (2022). Protein complex prediction with AlphaFold-Multimer. 2021.2010.2004.463034. 10.1101/2021.10.04.463034 %J bioRxiv.
119. Stiernagle T (2006). Maintenance of C. elegans. WormBook, 1–11. 10.1895/wormbook.1.101.1.
120. Lewis JA, and Fleming JT (1995). Basic culture methods. Methods Cell Biol 48, 3–29. [PubMed: 8531730]
121. König J, Zarnack K, Rot G, Curk T, Kayikci M, Zupan B, Turner DJ, Luscombe NM, and Ule J (2010). iCLIP reveals the function of hnRNP particles in splicing at individual nucleotide resolution. Nature Structural & Molecular Biology 17, 909–915. 10.1038/nsmb.1838.
122. Shirayama M, Seth M, Lee HC, Gu W, Ishidate T, Conte D Jr., and Mello CC (2012). piRNAs initiate an epigenetic memory of nonself RNA in the C. elegans germline. Cell 150, 65–77. 10.1016/j.cell.2012.06.015. [PubMed: 22738726]
123. Crittenden SL, Seidel HS, and Kimble J (2017). Analysis of the C. elegans Germline Stem Cell Pool. Methods Mol Biol 1463, 1–33. 10.1007/978-1-4939-4017-2_1. [PubMed: 27734344]
124. Lee C, Sorensen EB, Lynch TR, and Kimble J (2016). C. elegans GLP-1/Notch activates transcription in a probability gradient across the germline stem cell pool. Elife 5. 10.7554/eLife.18370.
125. Haupt KA, Law KT, Enright AL, Kanzler CR, Shin H, Wickens M, and Kimble J (2020). A PUF Hub Drives Self-Renewal in Caenorhabditis elegans Germline Stem Cells. Genetics 214, 147–161. 10.1534/genetics.119.302772. [PubMed: 31740451]

Author Manuscript Author Manuscript Author Manuscript Author Manuscript

Highlights

- A conserved PUF-partner interface modulates the *in vivo* PUF-RNA binding landscape.
- Partners can increase or reduce FBF-2 occupancy of specific sites in RNA targets.
- Partnerships can separate FBF-2 biological functions.
- FBF-2 partnerships drive a spatially patterned switch from repression to activation.

Author Manuscript Author Manuscript Author Manuscript Author Manuscript

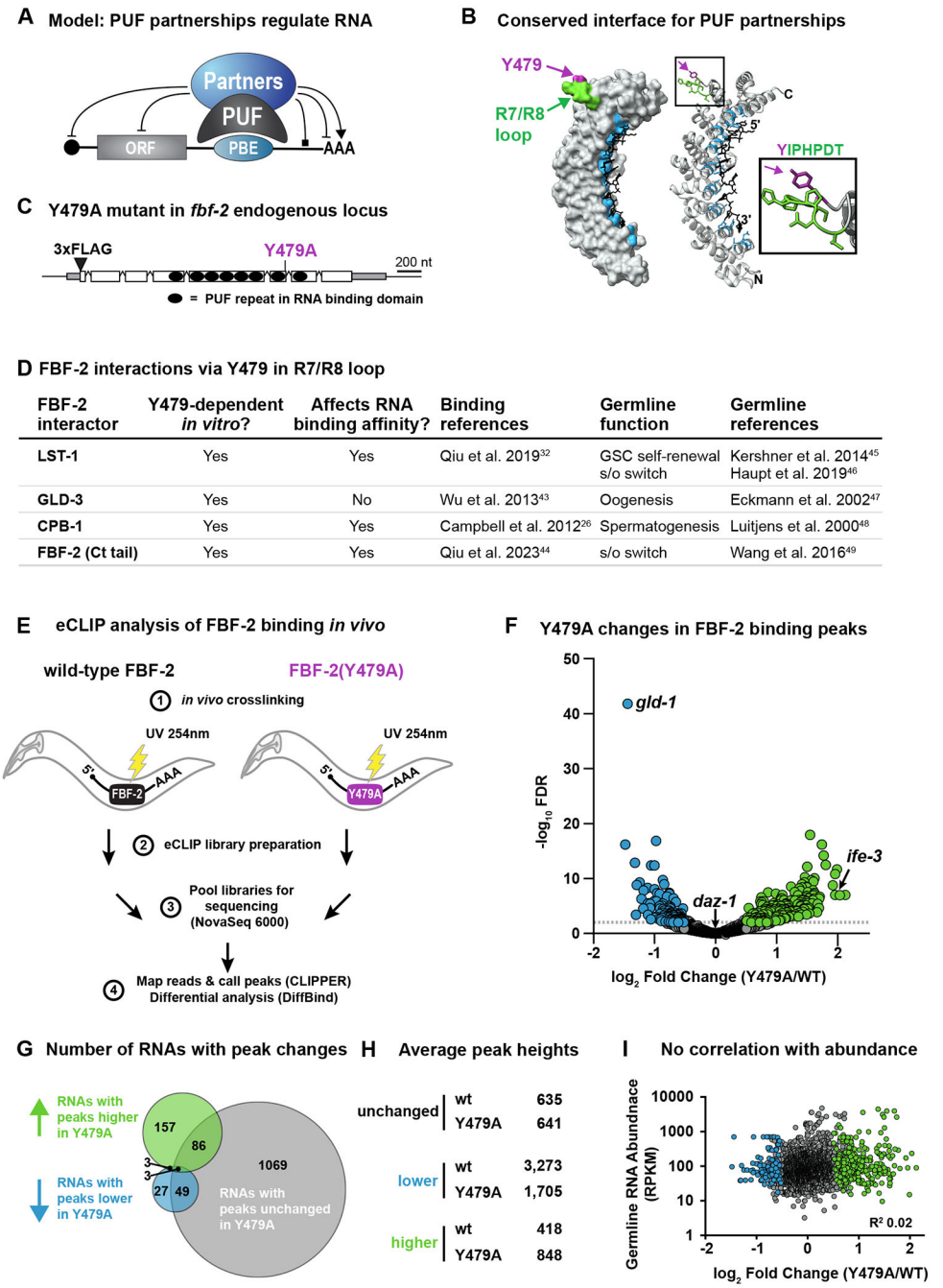

FBF-2 interactor	Y479-dependent *in vitro*?	Affects RNA binding affinity?	Binding references	Germline function	Germline references
LST-1	Yes	Yes	Qiu et al. 2019[32]	GSC self-renewal s/o switch	Kershner et al. 2014[45] Haupt et al. 2019[46]
GLD-3	Yes	No	Wu et al. 2013[43]	Oogenesis	Eckmann et al. 2002[47]
CPB-1	Yes	Yes	Campbell et al. 2012[26]	Spermatogenesis	Luitjens et al. 2000[48]
FBF-2 (Ct tail)	Yes	Yes	Qiu et al. 2023[44]	s/o switch	Wang et al. 2016[49]

Figure 1. Key tyrosine modulates the FBF-2 RNA-binding landscape.

(A) PUF proteins bind PUF binding elements (PBEs) and interact with partners to control mRNA. Arrowhead, activation; blunt end, repression; square end, RNA binding. (B) Crystal structure of FBF-2 (left, surface; right, ribbon; gray) binding to RNA (black) (PDB:3K5Y). RNA binding residues, blue; R7/R8 loop, green; Y479, purple. Inset focuses on R7/R8 residues. (C) *fbf-2* locus. Untranslated regions (gray boxes); coding regions (white boxes), introns (peaked lines), PUF repeats (black ovals). 3xFLAG and Y479 positions are indicated. D) Y479-dependent FBF-2 partners validated *in vitro* and their germline

Author Manuscript Author Manuscript Author Manuscript Author Manuscript

functions. Y479 dependence and effects on RNA binding affinity were determined using peptide fragments from partner proteins *in vitro*. (E) eCLIP workflow. (F) Comparison of wild-type FBF-2 and mutant FBF-2(Y479A) binding to individual peaks. Gray circle, RNA peak is same in wild-type and Y479A (gray becomes black with overlaps). Blue circle, RNA peak is lower in Y479A than wild-type. Green circle, RNA peak is higher in Y479A than wild-type. Dotted line marks FDR ≤0.01. Representative peak is labeled for each category. (G) Venn diagram showing overlap of RNAs harboring peaks in each category (colors as in Figure 1F). Numbers in main circles indicate number of RNAs with peaks in only one category; numbers in circle intersections indicate number of RNAs with peaks in different categories. (H) Average peak heights for wild-type and Y479A in all three categories. (I) Fold-changes in peaks of each category (x-axis, colors as in Figure 1F) are plotted as a function of germline RNA abundance (y-axis).

Author Manuscript
Author Manuscript
Author Manuscript
Author Manuscript

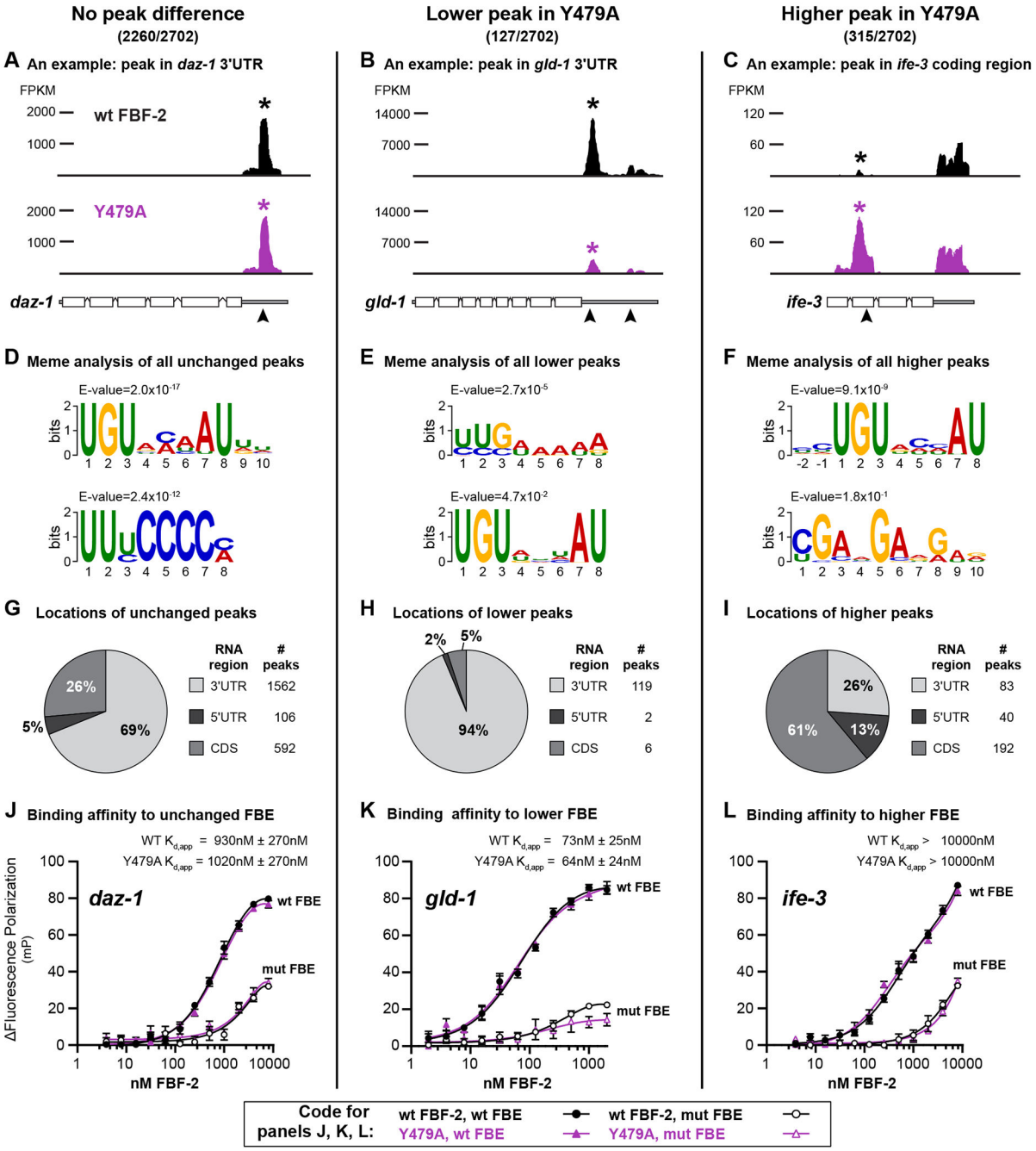

Figure 2. Peak features, category by category.

(A-C) Representative RNAs for each category, showing peak heights (above) and RNA positions (below). Peak heights are measured in fragments per kilobase mapped (FPKM) under the peak. Asterisks mark representative peaks. Black peak, wild-type; purple peak, Y479A. Arrowheads mark consensus FBEs under peaks. (A) *daz-1* peak with no difference in occupancy; (B) *gld-1* peak with lower occupancy in Y479A than wild-type; (C) *ife-3* peak with higher occupancy in Y479A than wild-type. (D-F) Top enriched motifs by MEME in each category. (G-I) Peak locations in each category. (J-L) RNA binding affinities for each

Author Manuscript Author Manuscript Author Manuscript Author Manuscript

category, assayed by fluorescence polarization. Error bars show standard error for triplicate measurements. Code shown below (wt, wild-type). $K_{d,app}$ is apparent K_d. See Figures S5A and S5B for protein and RNA info.

Author Manuscript Author Manuscript Author Manuscript Author Manuscript

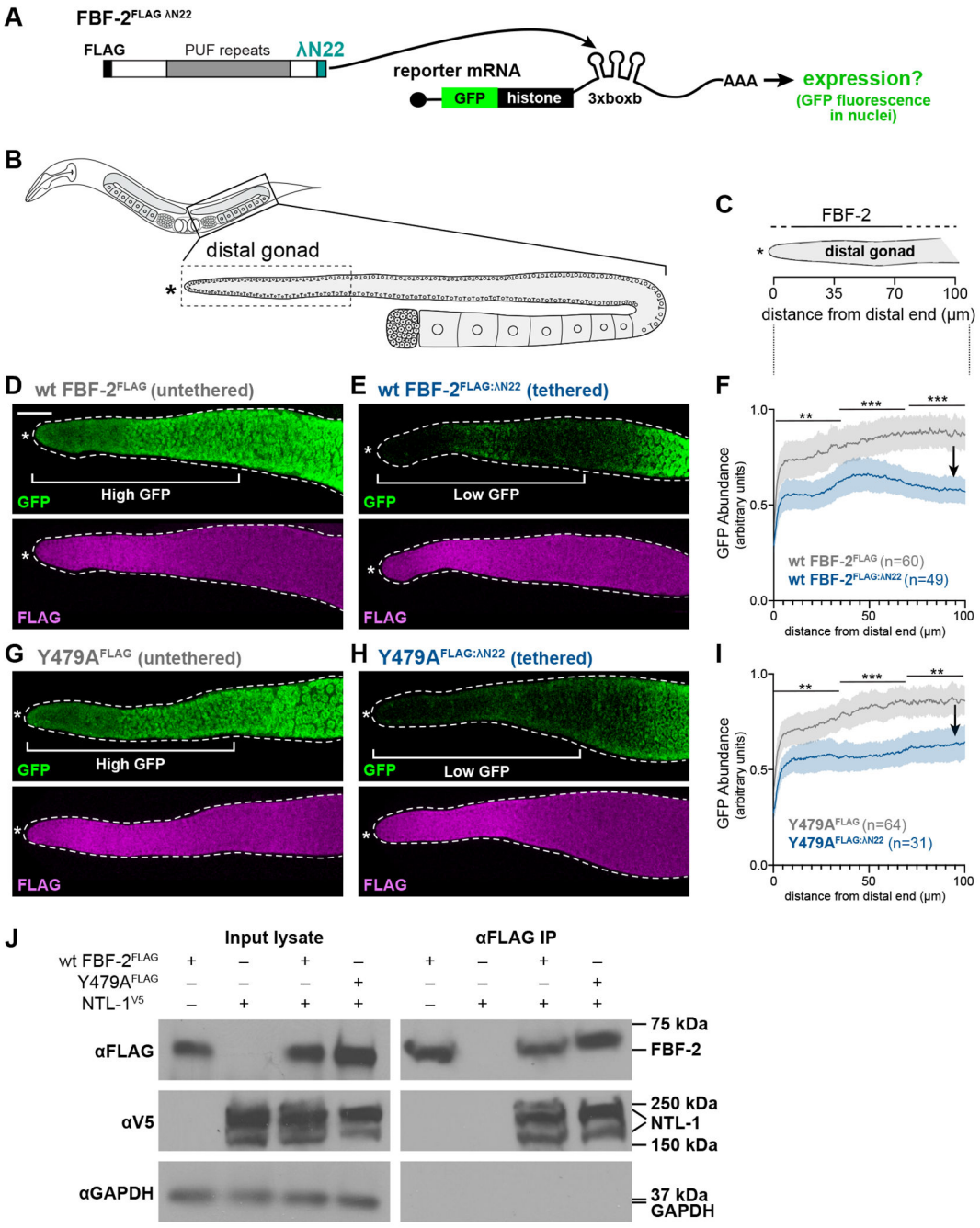

Figure 3. Y479A retains RNA repression activity.

(A) Tethering assay. FBF-2 is tethered by λN22 binding to boxB hairpins in the reporter RNA. Modified from Aoki et al. 2018[91]. (B) Above, location of gonadal arm (black box) within animal. Below, location of distal region (dotted box) within gonadal arm. Asterisk marks distal end. Germline stem cells (GSCs) reside at the most distal end of germline and their daughters begin differentiation as they move proximally. (C) Diagram of distal gonad, showing distance from the distal end in microns below and extents of abundant FBF-2 (black line) and lower FBF-2 (dotted line) above. (D-E) Representative z-projections

Author Manuscript Author Manuscript Author Manuscript Author Manuscript

of extruded germlines. 20μm scale bar in (D) applies to all images. Dotted line marks gonad boundary; asterisk marks distal end. Top, GFP reporter expression (green); bottom, FBF-2^{FLAG} staining (magenta). (D) Untethered wild-type FBF-2. (E) Tethered wild-type FBF-2. (F) ImageJ quantitation of reporter signal from tethered vs untethered FBF-2. GFP abundance plotted against distance from distal end. Solid line shows mean abundance and shading shows 95% confidence interval. Each plot represents three biological replicates with at least 10 gonad arms per replicate. P-values are given for pooled data in 0-35, 35-70 and 70-100 μm regions (black bars). P-values: *** $p < 0.001$, ** $p < 0.01$, * $p < 0.05$, ns (not significant) $p > 0.05$. Exact p-values in Table S4. (G-H) Representative z-projections of extruded germlines, as in (3D-E). (G) Untethered Y479A. (H) Tethered Y479A. (I) Quantitation of tethered vs untethered Y479A. P-values as in (F). (J) Western blots after FBF-2 and NTL-1 co-immunoprecipitation. Left, input lysates (1%); right, FLAG IP (10%). NTL-1:V5 co-immunoprecipitates with both wild-type and Y479A.

Author Manuscript Author Manuscript Author Manuscript Author Manuscript

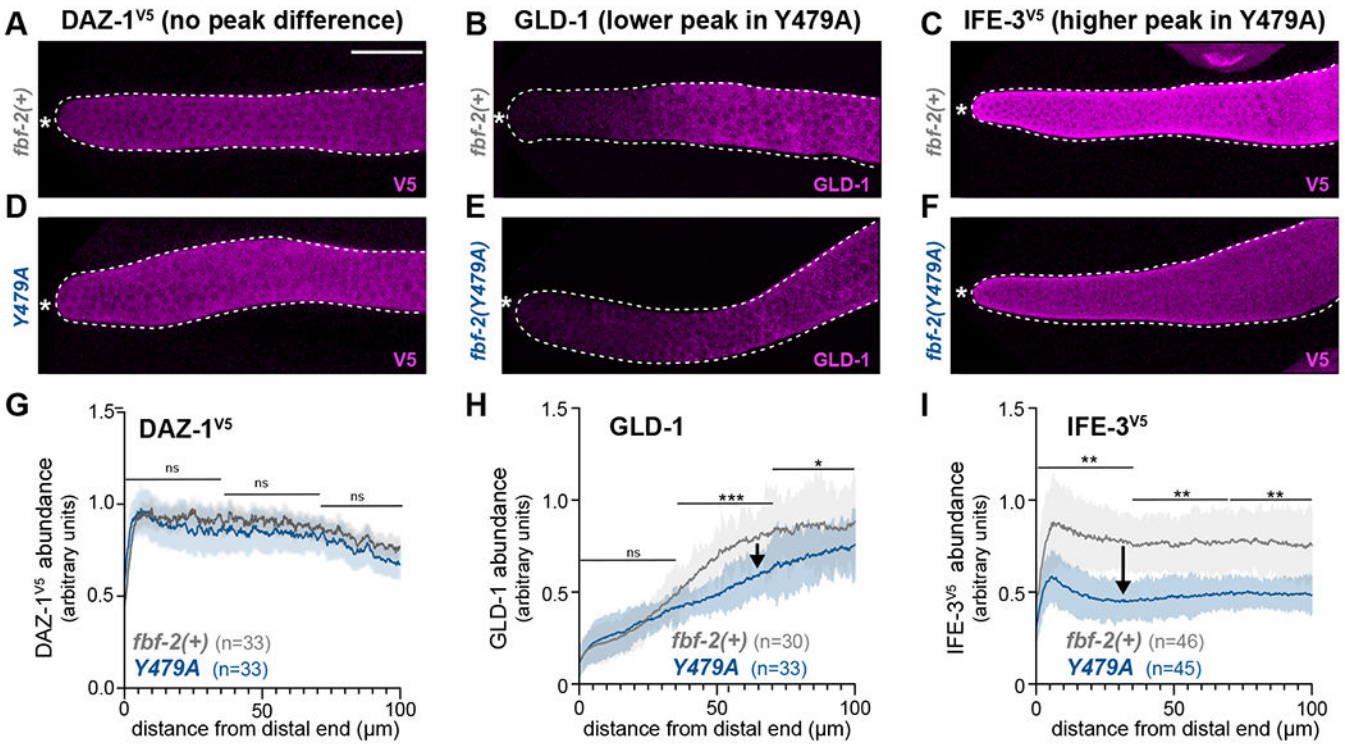

Figure 4. Y479A leads to RNA misregulation.

(A-F) Representative z-projections of stained extruded gonads. 20µm scale bar in (A) applies to (A-F). All images cropped at 100µm from distal end; dotted line marks gonad boundary; asterisk marks distal end. (A-C) Gonads with wild-type FBF-2; (D-F) gonads with Y479A. (G-I) Image J quantitation. Solid line shows mean abundance and shading shows 95% confidence interval. Each plot represents three biological replicates with at least 10 gonad arms per replicate. P-values are given for pooled data in 0-35, 35-70 and 70-100 µm regions (black bars). P-values: *** $p < 0.001$, ** $p < 0.01$, * $p < 0.05$, ns (not significant) $p > 0.05$. Exact p-values in Table S4. (G) DAZ-1 protein in wild-type and Y479A. (H) GLD-1 protein in wild-type and Y479A. (I) IFE-3 protein in wild-type and Y479A.

Author Manuscript Author Manuscript Author Manuscript Author Manuscript

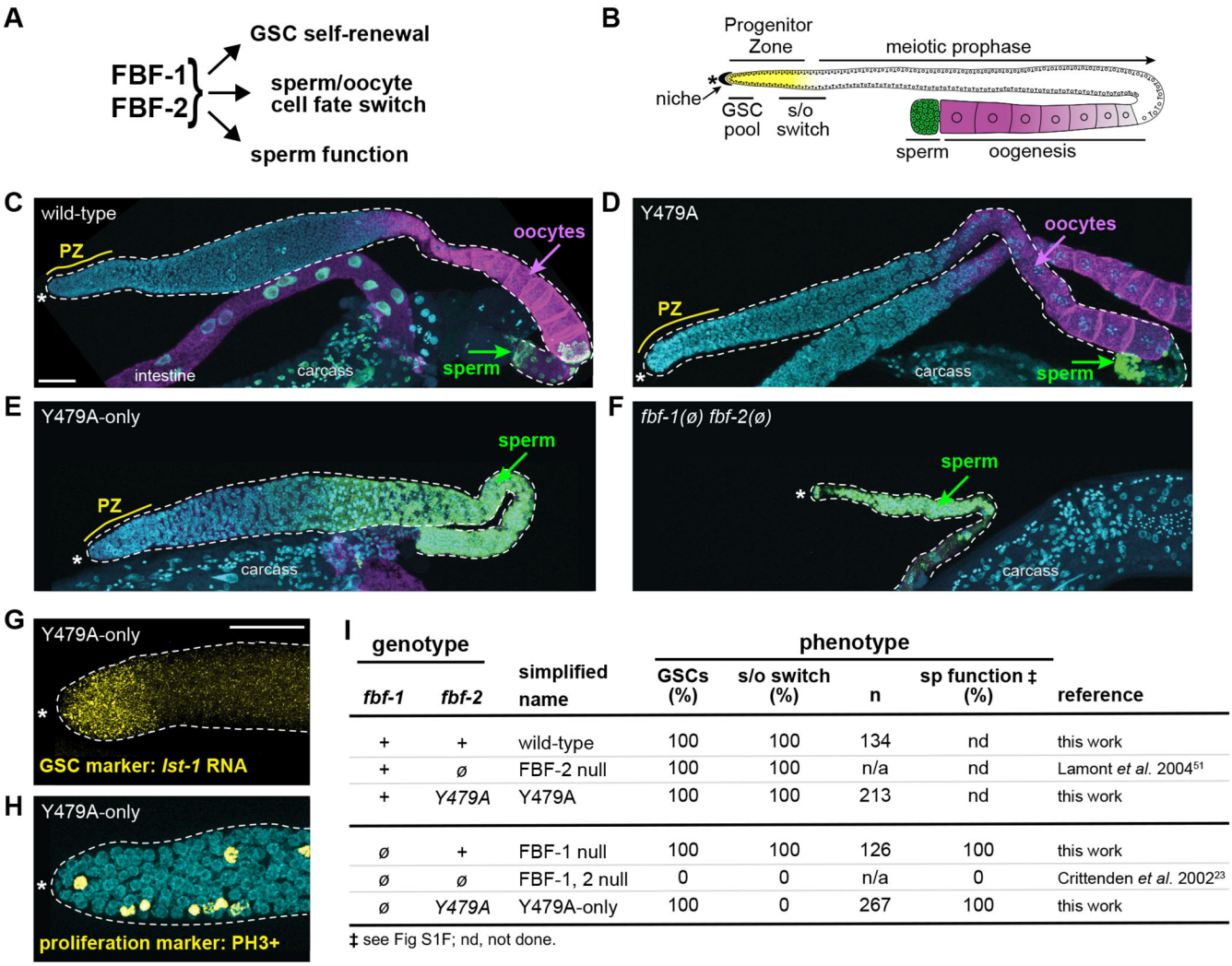

I

genotype			phenotype				
fbf-1	*fbf-2*	simplified name	GSCs (%)	s/o switch (%)	n	sp function ‡ (%)	reference
+	+	wild-type	100	100	134	nd	this work
+	ø	FBF-2 null	100	100	n/a	nd	Lamont *et al.* 2004[51]
+	*Y479A*	Y479A	100	100	213	nd	this work
ø	+	FBF-1 null	100	100	126	100	this work
ø	ø	FBF-1, 2 null	0	0	n/a	0	Crittenden *et al.* 2002[23]
ø	*Y479A*	Y479A-only	100	0	267	100	this work

‡ see Fig S1F; nd, not done.

Figure 5. Key FBF-2 tyrosine is required for the sperm to oocyte cell fate switch.

(A) FBF-1 and FBF-2 are redundant for three germline roles. GSC, germline stem cell. (B) Adult gonad organization. Progenitor Zone (PZ, yellow) includes a pool of GSCs adjacent to the distal end (asterisk) and GSC daughters making the sperm to oocyte cell fate switch (s/o switch) more proximally; mature sperm (green) are in spermatheca and oocytes develop in proximal arm (magenta). The distal end is capped by the stem cell niche. (C-F) Representative z-projection images of extruded adult gonads; stained for sperm (α-SP56, green), oocytes (α-RME-2, magenta) and DNA (DAPI, cyan). Dotted line marks gonad boundary; asterisk marks distal end; yellow line marks PZ extent. 20μm scale bar in (C) applies to (C-F) (G) Gonad stained by smFISH for lst-1 RNA, a GSC marker (yellow). 20μm scale bar in (G) applies to (G-H). (H) Gonad stained with α-phospho-histone H3 (PH3) to visualize M-phase chromosomes (yellow) and DAPI (cyan). (I) Y479A-only germline phenotype. GSCs, germline stem cells maintained; s/o switch, sperm to oocyte switch occurs, n, number gonads scored. See also Figure S6.

Author Manuscript Author Manuscript Author Manuscript Author Manuscript

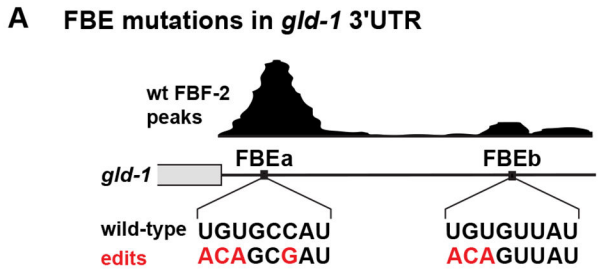

B *gld-1* FBE mutations affect germline fates

Genotype	Phenotype		
FBE	GSCs (%)	s/o switch (%)	n
+	100	100	216
a mut	99	97	700
b mut	100	100	980
ab mut	93	13	68

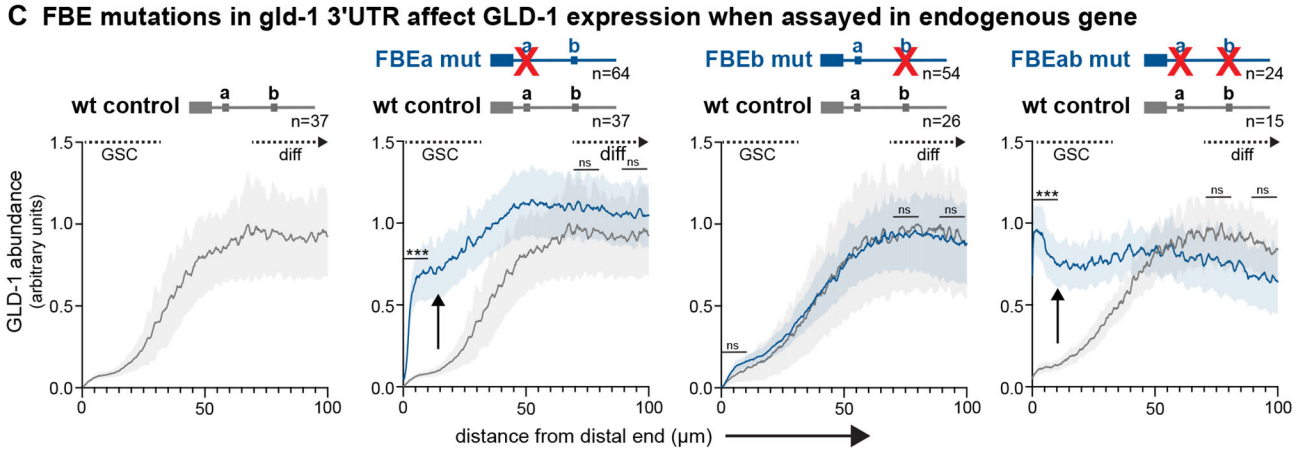

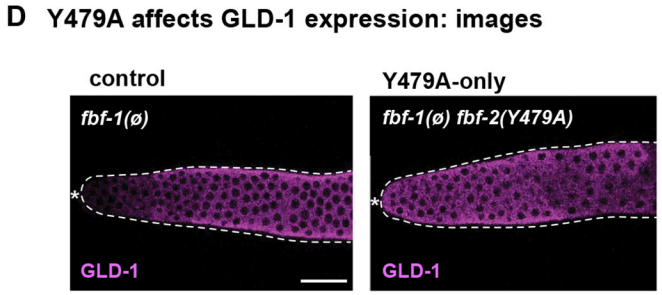

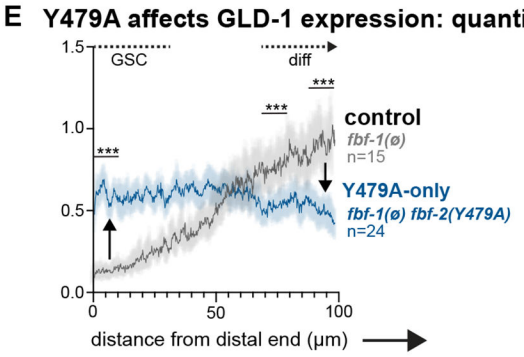

Figure 6. Effects of individual FBEs and Y479A on GLD-1 protein expression.

(A) Schematic of *gld-1* 3'UTR. Two consensus FBEs, FBEa and FBEb (black boxes), reside under two wild-type (wt) FBF-2 eCLIP peaks. Wild-type FBE sequences in black; mutations in red. (B) FBE mutations affect germline phenotypes. GSCs, germline stem cells are maintained; s/o switch, sperm to oocyte switch occurs successfully. FBE effects (red). n, number gonads scored. (C) Image J quantitation of GLD-1 abundance (y-axis) scored as a function of distance from the distal end (x-axis). Graph lines (wild-type, grey; FBE mutant, blue) show mean GLD-1 abundance. Shading is the 95% confidence interval. Compared gonads were processed and quantitated together. Dotted lines above graphs mark where the GSC pool (GSC) and entry into differentiation (diff) occur in wild-type gonads. P-values are given for pooled data in 0-10, 70-80 and 90-100 µm regions (black bars). P-values: *** $p < 0.001$, ** $p < 0.01$, * $p < 0.05$, ns (not significant) $p > 0.05$. Exact p-values in Table S4. (D-E) Images and quantitation of GLD-1 abundance in gonads with wild-type FBF-2

Author Manuscript Author Manuscript Author Manuscript Author Manuscript

and Y479A-only gonads (no FBF-1). (D) Representative z-projection images of GLD-1 in extruded germlines. Left, control gonad harbors no FBF-1 but has wild-type FBF-2 protein; right, Y479A-only gonad has no FBF-1 but has mutant Y479A protein. Scale bar 20μm (applies to both images). (E) Image J quantitation of GLD-1 abundance. Black line, abundance in control gonads; blue line, abundance in Y479A-only gonads. Conventions and p-values as in C. See also Figure S7.

Author Manuscript Author Manuscript Author Manuscript Author Manuscript

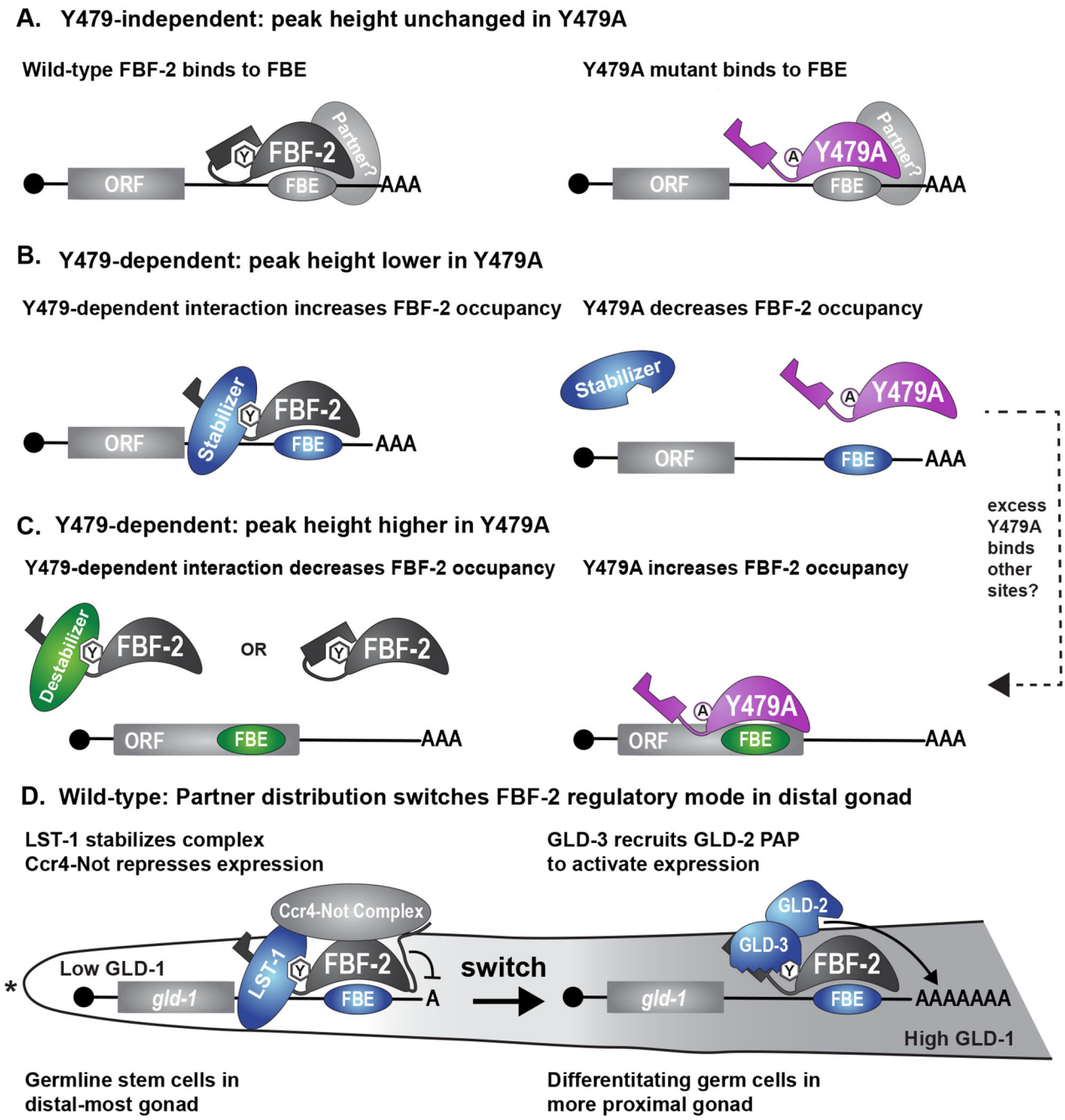

Figure 7. Models for Y479 effects on FBF binding landscape and regulatory mode.

(A-C) Models for how Y479-dependent interactions modulate FBF-2 occupancy. Target RNAs (straight lines) with a cap (circle) at 5' end, open reading frame (ORF) and 3' untranslated region (3'UTR). In each case, wild-type (left) and Y479A (right) diagrams represent extremes of the likely spectrum of possibilities. Partners are color-coded according to effects on FBF-2 occupancy (grey, no change in Y479A; blue, lower in Y479A; green, higher in Y479A), and FBEs are similarly color-coded according to Y479-dependent effects (grey, no change in Y479A; blue, lower in Y479A; green, higher in Y479A). (A) Peak

Author Manuscript Author Manuscript Author Manuscript Author Manuscript

unchanged by Y479A (most in 3'UTR). Left: Wild-type FBF-2 binds to an FBF binding element (FBE) (grey) independently of interactions at Y479. Right: Y479A occupancy is unchanged. (B) Peaks lowered by Y479A (most in 3'UTR). Left: Wild-type FBF-2 interacts via Y479 with stabilizing partner (blue) to increase its FBE occupancy. Right: Y479A mutant protein does not interact with stabilizing partner so its FBE occupancy decreases. (C) Peaks increased by Y479A (most in coding regions). Left: Wild-type FBF-2 interacts via Y479 with destabilizing partner (green) or its own autoinhibitory C-terminal tail, either of which lowers FBE occupancy. Right: Y479A mutant protein occupies the FBE (green), due to release from its destabilizing partner or release from its autoinhibitory C-terminal tail. In addition, excess Y479A protein, released from sites that are high occupancy in wild-type, binds to sites that are low occupancy in wild-type (dotted arrow from 7B to 7C). (D) Diagram of Y479-dependent spatial regulation of *gld-1* mRNA in the wild-type distal gonad. The distal to proximal axis of the gonad is oriented from left to right with an asterisk at the distal end. We propose that LST-1 stabilizes FBF-2 interactions with *gld-1* FBEs in the distal-most gonad, allowing repression by the Ccr4-Not complex (low GLD-1, white fill in gonad), and that FBF-2 partnerships exchange as germ cells move proximally where the GLD-2/3 heterodimer promotes *gld-1* activation (high GLD-1, dark grey fill in gonad).

Author Manuscript Author Manuscript Author Manuscript Author Manuscript

KEY RESOURCES TABLE

REAGENT or RESOURCE	SOURCE	IDENTIFIER
Antibodies		
mouse monoclonal αFLAG M2	Sigma-Aldrich	Cat# F1804, RRID:AB_262044
mouse monoclonal αGFP 3E6	Thermo Fisher Scientific	Cat# A-11120, RRID:AB_221568
mouse monoclonal αV5	Bio-Rad	Cat# MCA1360, RRID:AB_322378
rabbit polyclonal αGLD-1	Betsy Goodwin (Jan et al., 1999)[87]	N.A.
mouse monoclonal αSP56	Sam Ward (Ward et al., 1986)[88]	N.A.
rabbit polyclonal αRME-2	Barth Grant (Grant and Hirsh, 1999)[89]	N.A.
mouse monoclonal αPH3	Cell Signaling Technology	Cat# 9706, RRID:AB_331748
mouse monoclonal αGAPDH	Proteintech	Cat# 60004-1-Ig, RRID:AB_2107436
donkey polyclonal αMouse-Alexa647	Molecular Probes/Invitrogen	Cat# A-31571, RRID:AB_162542
donkey polyclonal αRabbit-Alexa 488	Molecular Probes/Invitrogen	Cat# A-21206, RRID:AB_2535792
goat polyclonal αMouse-HRP	Jackson ImmunoResearch Labs	Cat# 115-035-003, RRID:AB_10015289
Bacterial and Virus Strains		
E. coli: OP50	Caenorhabditis Genetics Center (CGC)	RRID:WB-STRAIN:WBStrain00041969
E. coli: OP50-1 (Streptomycin resistant OP50)	Caenorhabditis Genetics Center (CGC)	RRID:WB-STRAIN:WBStrain00041971
E. coli: DH5α Competent Cells	Thermo Fisher Scientific	Cat# 18265017
E. coli: BL21(DE3) Competent Cells - Novagen	Millipore Sigma	Cat# 69450
Chemicals, Peptides, and Recombinant Proteins		
Alt-R™ S.p. Cas9 V3, glycerol-free	IDT	Cat# 10007806
cOmplete™, EDTA-free Protease Inhibitor Cocktail	Millipore Sigma	Cat# 04693132001
Benzonase® Nuclease, ultrapure	Millipore Sigma	Cat# E8263-25KU
Deposited Data		
Raw & processed eCLIP files (wild-type FBF-2 and FBF-2(Y479A))	This study	GEO accession GSE233561
Experimental Models: Organisms/Strains		
C. elegans: N2: wild-type	Caenorhabditis Genetics Center (CGC) (Brenner, 1974)[90]	RRID:WB-STRAIN:WBStrain00000001
C. elegans: EG8081: *unc-119(ed3) III; oxTi177 IV*	Caenorhabditis Genetics Center (CGC) (Frøkjær-Jensen et al 2014)[91]	RRID:WB-STRAIN:WBStrain00006964
C. elegans: JK3022: *fbf-1(ok91[null]) II*	Crittenden et al. 2002[23]	RRID:WB-STRAIN:WBStrain00022603
C. elegans: JK3101: *fbf-2(q738[null]) II*	Lamont et al. 2004[51]	RRID:WB-STRAIN:WBStrain00022611
C. elegans: JK3107: *fbf-1(ok91[null]) fbf-2(q704[null]) / mIn1 [mIs14 dpy-10(e128)] II*	Crittenden et al. 2002[23]	RRID:WB-STRAIN:WBStrain00022612

Author Manuscript Author Manuscript Author Manuscript Author Manuscript

REAGENT or RESOURCE	SOURCE	IDENTIFIER
C. elegans: JK4266: *fog-3(q520[null]) / hT2[qIs48] (I;III)*	Ellis and Kimble 1995[92]	N.A.
C. elegans: JK4864: *qIs147[sur-5::gfp] IV*	Lynch et al. 2022[93]	N.A.
C. elegans: JK5032: *fbf-1(ok91[null]) fbf-2(q704[null]) qSi75[3xflag::fbf-2] II*	Prasad & Porter et al. 2016[20]	N.A.
C. elegans: JK5800: *qSi364[3xflag::fbf-2(ΔY479-T485)] IV*	This study	N.A.
C. elegans: JK5810: *fbf-2(q945[3xflag::fbf-2]) II*	Ferdous et al. 2023[31]	N.A.
C. elegans: JK5833: *fbf-1(ok91[null]) fbf-2(q704[null]) / mIn1 [mIs14 dpy-10(e128)] II; qSi364[3xflag::fbf-2(ΔY479-T485)] IV*	This study	N.A.
C. elegans: JK5935: *fbf-1(ok91[null]) fbf-2(q973[3xflag::fbf-2]) II*	This study	N.A.
C. elegans: JK5984: *fbf-2(q1011[3xflag::fbf-2(Y479A)]) II*	This study	N.A.
C. elegans: JK5986: *fbf-1(ok91[null]) fbf-2(q1023[3xflag::fbf-2(Y479A)]) / mIn1 [mIs14 dpy-10(e128)] II*	This study	N.A.
C. elegans: JK6332: *lst-1(q1004[3xV5]) I; glp-1(ar202[gf]) III*	Ferdous et al. 2023[31]	N.A.
C. elegans: JK6367: *qSi375[(mex-5p::eGFP::linker::his-58::3xboxb::tbb-2 3'UTR) *weSi2] II*	Aoki et al. 2018[60]	N.A.
C. elegans: JK6373: *fbf-2(q945[3xflag]) II; glp-1(ar202[gf]) III*	Ferdous et al. 2023[31]	N.A.
C. elegans: JK6374: *lst-1(q1004[3xV5]) I; fbf-2(q945[3xflag]) II; glp-1(ar202[gf]) III*	Ferdous et al. 2023[31]	N.A.
C. elegans: JK6410: *fbf-2(q1078[3xflag::fbf-2::λN22]) II*	This study	N.A.
C. elegans: JK6412: *fbf-2(q1080[3xflag::fbf-2(Y479A)::λN22]) II*	This study	N.A.
C. elegans: JK6489: *lst-1(q1004[3xV5]) I; fbf-2(q1011[3xflag,Y479A]) / mIn1 [mIs14 dpy-10(e128)] II; glp-1(ar202[gf]) III*	This study	N.A.
C. elegans: JK6526: *ntl-1(q1238[ntl-1::1xV5]) III*	This study	N.A.
C. elegans: JK6540: *gld-1(q1242[FBEa mut]) I / hT2[qIs48] (I;III)*	This study	N.A.
C. elegans: JK6551: *fbf-2(q945[3xflag::fbf-2]) II; ntl-1(q1238[ntl-1::1xV5]) III*	This study	N.A.
C. elegans: JK6552: *fbf-2(q1011[3xflag::fbf-2(Y479A)]) II; ntl-1(q1238[ntl-1::1xV5]) III*	This study	N.A.
C. elegans: JK6563: *daz-1(q1254[1xV5::daz:1]) II*	This study	N.A.
C. elegans: JK6564: *daz-1(q1255[1xV5::daz:1]) fbf-2(q945[3xflag::fbf-2]) II*	This study	N.A.
C. elegans: JK6565: *daz-1(q1256[1xV5::daz:1]) fbf-2(q1011[3xflag::fbf-2(Y479A)]) II*	This study	N.A.
C. elegans: JK6568: *gld-1(q1257[FBEb mut]) I*	This study	N.A.
C. elegans: JK6594: *ife-3(q1259[1xV5::ife-3]) V*	This study	N.A.
C. elegans: JK6602: *gld-1(q1271[FBEab mut]) I / hT2[qIs48](I;III)*	This study	N.A.
C. elegans: JK6605: *fbf-2(q945[3xflag::fbf-2]) II; ife-3(q1259[1xV5::ife-3]) V*	This study	N.A.

Author Manuscript Author Manuscript Author Manuscript Author Manuscript

REAGENT or RESOURCE	SOURCE	IDENTIFIER
C. elegans: JK6606: *fbf-2(q1011[3xflag::fbf-2(Y479A)]) II; ife-3(q1259[1xV5::ife-3]) V*	This study	N.A.
C. elegans: JK6615: *fbf-2(q945[3xflag::fbf-2]) II; qIs147[sur-5::gfp] IV*	This study	N.A.
C. elegans: JK6616: *daz-1(q1255[1xV5::daz:1]) fbf-2(q945[3xflag::fbf-2]) II; qIs147[sur-5::gfp] IV*	This study	N.A.
C. elegans: JK6617: *fbf-2(q945[3xflag::fbf-2]) II; qIs147[sur-5::gfp] IV; ife-3(q1259[1xV5::ife-3]) V*	This study	N.A.
C. elegans: JK6690: qSi422[(*gld-1p::GFP::H2B::gld-1 3′UTR(FBEa mut) + Cbr-unc-119(+)) *rajSi50] II; unc-119(ed3) III*	This study	N.A.
C. elegans: JK6692: qSi424[(*gld-1p::GFP::H2B::gld-1 3′UTR(FBEb mut) + Cbr-unc-119(+)) *rajSi50] II; unc-119(ed3) III*	This study	N.A.
C. elegans: JK6693: qSi425[(*gld-1p::GFP::H2B::gld-1 3′UTR(FBEab mut) + Cbr-unc-119(+)) *rajSi50] II; unc-119(ed3) III*	This study	N.A.
C. elegans: JK6694: *rajSi50[gld-1p::GFP::H2B::gld-1 3′UTR + Cbr-unc-119(+)] II; unc-119(ed3) III*	Theil et al. 2013[66]	N.A.
Oligonucleotides		
DNA Oligos (IDT)	See Table S6 for sequences and use.	
Software and Algorithms		
FastQC: v. 0.11.9	http://www.bioinformatics.babraham.ac.uk/projects/fastqc/	FastQC (RRID:SCR_014583)
Cutadapt: v. 1.18	Martin 2011[94]	cutadapt (RRID:SCR_011841)
STAR: v. 2.7.2a	Dobin et al. 2013[95]	STAR (RRID:SCR_004463)
Samtools: v. 1.9	Li et al. 2009[96]	SAMTOOLS (RRID:SCR_002105)
bedToBigBed: v. 2.5	https://genome.ucsc.edu	N.A.
Bedtools: v. 2.28.0	Quinlan & Hall 2010[97]	BEDTools (RRID:SCR_006646)
MEME v 5.3.3, Tomtom v 5.5.2	Bailey & Elkan 1994[98], Gupta et al. 2007[99]	MEME Suite - Motif-based sequence analysis tools (RRID:SCR_001783)
Python 2.7.18	Van Rossum & Drake 1995[100]	Python Programming Language (RRID:SCR_008394)
Pysam 0.15.3	https://github.com/pysam-developers/pysam	pysam (RRID:SCR_021017)
bx-python 0.8.4	https://github.com/bxlab/bx-python	N.A.
HTSeq 0.6.1p1	Anders et al. 2015[101]	HTSeq (RRID:SCR_005514)
NumPy 1.16.4	https://github.com/numpy/numpy	NumPy (RRID:SCR_008633)
Pandas 0.24.2	https://github.com/pandas-dev/pandas	Pandas (RRID:SCR_018214)
Pybedtools 0.8.0	http://daler.github.io/pybedtools/	pybedtools (RRID:SCR_021018)
scikit-learn 0.20.4	Pedregosa et al. 2011[102]	scikit-learn (RRID:SCR_002577)
SciPy 1.2.1	Virtanen et al. 2020[103]	SciPy (RRID:SCR_008058)

Author Manuscript Author Manuscript Author Manuscript Author Manuscript

REAGENT or RESOURCE	SOURCE	IDENTIFIER
Matplotlib 2.2.4	Hunter 2007[104]	MatPlotLib (RRID:SCR_008624)
GFFUtils 0.9	https://github.com/fls-bioinformatics-core/GFFUtils	N.A.
Seaborn 0.9.0	Waskom 2021[105]	seaborn (RRID:SCR_018132)
statsmodels 0.10.1	Seabold et al 2010	statsmodel (RRID:SCR_016074)
R 3.0.2	https://www.r-project.org/	R Project for Statistical Computing (RRID:SCR_001905)
tidyselect 1.1.1	https://tidyselect.r-lib.org	N.A.
readxl 1.3.1	https://readxl.tidyverse.org	readxl (RRID:SCR_018083)
seqLogo 1.56.0	https://bioconductor.org/packages/release/bioc/html/seqLogo.html	N.A.
DiffBind 3.0.15	Stark & Brown 2011[55]	DiffBind (RRID:SCR_012918)
ChIPseeker 1.26.2	Yu et al. 2015[106]	ChIPseeker (RRID:SCR_021322)
GenomicFeatures 1.42.3	Lawrence et al. 2013[107]	GenomicFeatures (RRID:SCR_016960)
BSgenome.Celegans.UCSC.ce10 1.4.0	https://bioconductor.org/packages/release/data/annotation/html/BSgenome.Celegans.UCSC.ce10.html	N.A.
Perl 5.26.2	Wall & Orwant 2000[108]	Perl Programming Language (RRID:SCR_018313)
Statistics-Distributions 1.02	https://metacpan.org/pod/Statistics::Distributions	N.A.
Barcode_collapse_pe.py	https://github.com/YeoLab/gscripts/releases/tag/1.1	N.A.
Make_bigwig_files.py	https://github.com/YeoLab/gscripts/releases/tag/1.1	N.A.
Clipper	https://github.com/YeoLab/clipper/releases/tag/1.1	N.A.
Clip_analysis	https://github.com/YeoLab/clipper/releases/tag/1.1	N.A.
negBedGraph.py	https://github.com/YeoLab/gscripts/releases/tag/1.1	N.A.
demux_paired_end.py	https://github.com/YeoLab/gscripts/releases/tag/1.1	N.A.
fastq-sort	https://github.com/dcjones/fastq-tools	N.A.
Peak_input_normalization_wrapper.pl	https://github.com/YeoLab/gscripts/tree/1.1/perl_scripts	N.A.
overlap_peakfi_with_bam_PE.pl	https://github.com/YeoLab/gscripts/tree/1.1/perl_scripts	N.A.
compress_l2foldenrpeakfi.pl	https://github.com/YeoLab/gscripts/tree/1.1/perl_scripts	N.A.